Electrospun Pretreatment Membranes

by

Husain Mithaiwala

A Thesis Presented in Partial Fulfillment
of the Requirements for the Degree
Master of Science

Approved July 2020 by the
Graduate Supervisory Committee:

Matthew Green, Chair
Lenore Dai
Julianne Holloway

ARIZONA STATE UNIVERSITY

August 2020

ABSTRACT

Managing water resources has become one of the most pressing concerns of scientists both in academia and industry. The reverse osmosis (RO) water treatment process is a well-researched technology among the pressure driven processes to produce potable water. RO is an energy intensive process and often RO membranes are susceptible to fouling and scaling that drives up operational cost and hinder the efficiency. To increase the performance of RO membranes the feed water is pretreated to remove pollutants before desalination. This work aims to fabricate pretreatment membranes to prevent the effects of fouling and scaling by introducing hydrophilic character to membrane. This work explores electrospinning, a cost-effective and scalable technique, to blend two polymers into a nonwoven membrane comprised of fibers ~100 nm - 10 μm in diameter.

A rotary drum collector holding the mat was used to simultaneously collect the electrospun hydrophobic poly(vinyl chloride) (PVC) and hydrophilic poly(vinyl alcohol) (PVA) fibers from two separate solutions. The hydrophilicity of the resulting membrane was tuned by controlling the relative deposition rate of PVA onto the co-spun mat. Fiber diameter and morphologies were characterized by scanning electron microscopy, and Fourier-transform infrared spectroscopy and Confocal fluorescence microscopy further confirmed the presence of both polymers. Moreover, a rigorous analysis to map the PVA/PVC concentration was established to accurately report the relative concentrations of the two polymers on the co-spun mat. After electrospinning, the PVA in the co-spun mats were cross-linked with poly(ethylene glycol) diacid to impart mechanical strength and tune the porosity.

EDS analysis revealed inconsistencies in the mass deposition of both polymers suggesting an improvement in the current experimental design to establish a meaningful relationship between PVA concentration and hydrophilicity. However, tensile test revealed that co-spun mats with high mass flow ratios of PVA possessed high mechanical strength showing a significant improvement in the Young's Modulus. Furthermore, the co-spun mats were challenged with filtration experiments expecting a positive correlation of flux with PVA concentration. But it was found that with increased concentration, crosslinked PVA constricted PVC fibers minimizing the pores causing a lower flux and a dense membrane structure suitable for filtration.

DEDICATION

To my parents

Imtiaz Taherali Mithaiwala

Maleka Abbasali Mithaiwala

ACKNOWLEDGMENTS

This thesis would not have been possible without the support and encouragement of many people. First, I would like to thank my graduate supervisory committee who took out the time for supervising my work. I would especially like to thank my supervisor, Dr. Matthew Green, for his guidance and support through each stage of the process and for always believing in me. I convey my genuine gratitude to Mani, for his direction, encouragement and support during this project. I would like to thank all fellow research group members for their constant enthusiasm.

Finally, I would like to thank my family and friends for always being there. Your love and laughter kept me smiling and inspired.

TABLE OF CONTENTS

Page

CHAPTER Page

LIST OF TABLES

Table Page

LIST OF FIGURES

Figure Page

Figure Page

LIST OF SYMBOLS

Symbol Page

CHAPTER 1

INTRODUCTION

A study conducted a decade ago found that there are over 1 billion people without access to clean drinking water and approximately 2.3 billion reside in regions with water shortages (Service, 2006; Lauren et. al, 2009). According to the U.S Geological survey, seas and oceans account for 96.5% of earth's water and ice caps account for 1.7%, and approximately 0.8% existing as freshwater (Gleick, 1996). The remaining percentage comprises of brackish water, and salty water trapped in estuaries and salty aquifers. The demand for fresh water exceeds multifold times than the supply i.e. the rate of consumption is much higher than the rate of production. Additionally, the freshwater sources such as lakes, rivers, and groundwater are diminishing or becoming saline. These issues stem the need of water reuse and water desalination as a solution to sustain the water resources for future generation across the globe.

Thermal desalination and membrane technology are two of the most promising technologies developed in the recent past available to convert saline water to potable water. The process of thermal desalination has been adapted for hundreds of years for producing fresh water, but large-scale production for municipal treatment was not adapted until 1950s (Gleick,2006). This technology is majorly concentrated in the Middle east countries, who have pioneered the design, and implementation of seawater thermal desalination and collectively holds around 50% of the world's desalination capacity (Lauren et. al, 2009). Although thermal desalination was implemented at large scale in the middle east, membrane processes started getting widely adapted worldwide because of their less specific energy requirement (Geoffrey et. al 2013; Semiat R, 2008; Anderson MA et. al

2005). In 2001, 51% of new installed desalination capacities used membrane-based technology (reverse osmosis) and in 2003, it accounted for 75% of new production capacity outside of the Middle East (Wolfe, 2005). Recently, membrane technology has become one of the most promising ways to produce high quality (Lin et al., 2016; Ochando-Pulido et al., 2016; Tang et al., 2016b).

Membrane Based Separation Processes

Microfiltration (MF), ultrafiltration (UF), nanofiltration (NF), reverse osmosis (RO), forward osmosis (FO), and membrane distillation (MD) are some of the common membrane processes for water purification and desalination. These processes are classified based on the size (referring to the diameter) of the solutes retained. Generally, MF membranes remove suspended particles and microbial pathogens, UF membranes retain macromolecules, like natural organic matter (NOM), smaller pathogens such as viruses that are partially removed by MF. MF and UF membranes are porous in nature, and separation is governed on sieve or size exclusion mechanism. NF membranes can remove scale-forming ions, such as calcium and magnesium, and considerably reduce salinity. Whereas, RO and FO are dense membranes designed for desalination capable of removing ions in addition to uncharged solutes. The molecular transport in RO and FO is based on solution-diffusion mechanism, and separation in NF is based on both sieving and solution diffusion mechanism. Additionally, the molecular weight cut-off in UF membrane is between 5-500 kDa, NF membranes between 100-300 Da, and RO and FO membranes is around 100 Da. Figure 1 gives an overview of membrane treatment processes for water purification and desalination with nominal pore size ranges and contaminant retaining capabilities. (Werber, J et. al, 2016)

Among the above-mentioned membrane process, RO membrane technology is recognized as a promising and optimized technology for converting saline water to potable water and meet the global demands (Lee et. al, 2011). It is estimated that there are over 15,000 desalination plants worldwide, of which RO accounts for approximately 50% of them.

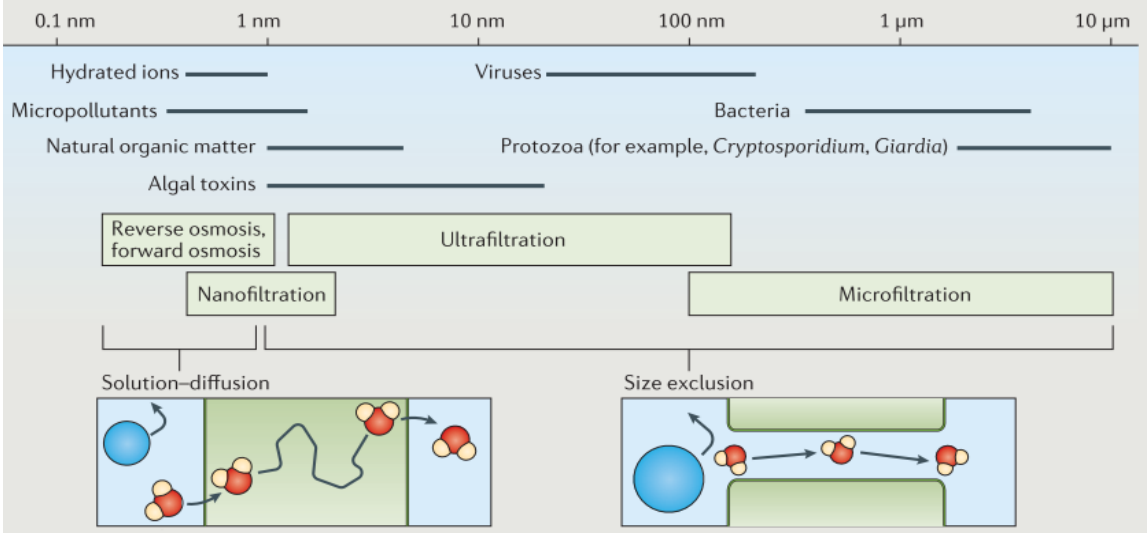

Figure 1. Membrane processes for water purification and desalination (Werber, J et. al, 2016).

Reverse Osmosis

RO is a pressure-driven process where, a semi-permeable membrane (RO membrane) restricts the constituents from the feed water, meanwhile allowing the water to pass through (Kang et.al, 2012). This is typically done by applying external pressure to overcome the osmotic pressure to force the water through the membrane to reach the permeate side. The concept of RO has been existent for a long time now, but the use of RO as a viable separation process was only possible due to the recent developments of RO membranes, that determines the economic and technological efficiency of RO process

(Kang et.al, 2012). RO membranes can restrict smallest contaminants, monovalent ions such as chlorine, sodium (98-99.8% rejection) (Bartels et. al, 2005), while other membranes, like NF exhibit rejection of 60-70% of monovalent ions (Choi et al, 2001; Hilal et. al, 2004), UF and MF are designed to remove contaminants of increasing size (Lauren et. al, 2009).

The two key parameters for RO membranes are water flux and salt rejection. In theory, these membranes should possess high salt rejection and high flux. Additionally, they should have mechanical durability, chlorine tolerant, foulant resistant and low cost (Li et. al, 2010). RO membranes are generally operated in crossflow filtration mode and are available as spiral wound modules, where an inner tube that collects the permeate is wrapped around membrane sheets (Baker, 2004). The filtration is allowed through pores and the fluid flow is dependent on the membrane porosity, fraction of volume available as void space within the membrane and tortuosity. Furthermore, the fluid flux also occurs due to diffusion and as mentioned above RO transport mechanism has been termed solution-diffusion (Lonsdale et al., 1965; Merten, 1963; Paul, 1972, 2004; Wijmans and Baker, 1995).

Conventionally, the performance of a RO unit is indicated by the recovery, which is defined as the ratio of permeate volumetric flow rate and feed volumetric flow rate. The recovery varies from 35% to 85%, depending on the composition of feed water, pretreatment techniques, and optimum energy design configuration (Lauren. et. al, 2009). A variation in the recovery is directly associated with the overall cost of RO system, and the extent of limiting factors, such as fouling propensity, osmotic pressure and mineral scaling (Morenski, 1992; Wilf and Klinko, 2001). A higher recovery requires an increase

in permeate flux, feed pressure and membrane area. In the case of increase permeate flux, permeate salinity concentration decreases due to increase in dilution. Whereas, RO modules operated under higher permeate flux lead to flux decline, and when operated at higher recovery without changing the flux increases salt passage (Wilf and Kinko, 2001). Therefore, RO systems should be optimized based on the characteristic feed water, operating conditions and make design modifications to achieve a target recovery.

The accumulation of dissolved ions at the surface of the membrane during the RO operation results in a thin film giving rise to concentration polarization. RO units operated under any recovery, feed to this concentration polarization increasing the salt permeation through the membrane (Kim and Hoek, 2005; Song and Elimelech, 1995). An increase in the salinity concentration at the surface increases the osmotic pressure, consequently, an overall increase in the pressure (difference between hydrostatic and osmotic pressure) decreasing the permeate flow, while creating passage for salt transport through the passage (Lauren et. al 2009). This condition acts as stimulus to phenomena such as salt precipitation and fouling increase due to higher local salinity. There are several studies that demonstrate the calculation of actual salt concentration at the RO membrane surface (Bacchin et al., 2002; Gekas and Hallstro¨m, 1987; Kim and Hoek, 2005; Sutzkover et al., 2000; Zydney, 1997).

RO technology is widely adapted due to the recent process improvements and advances to reduce operational cost and energy consumptions. These advances have mainly focused on membrane properties, module design, process design, feed pretreatment, energy recovery devices and operational strategies (Penña et al. 2012). However, one of the major challenges for an efficient operation of RO facility is fouling. The consequence of fouling

phenomena on membrane systems is significant reduction of productivity and permeate quality that increases the operation cost due to high energy demand. In addition, requires further pretreatment, foulant removal, membrane cleaning, maintenance and reduction in membrane life expectancy. (Al-Amoudi, 2010; Eric et al., 2001; Kochkodan et al., 2014; Tang et al., 2011). In the past, several studies have focused on understanding the mechanism of fouling in membrane-based separation techniques (Giglia and Straeffer, 2012; Lee et al., 2015b; Mirbagheri et al., 2015; Tan et al., 2016). According to statistical analysis, data reveals that there are over 3000 papers published in the last 25 years to address the issue of RO membrane fouling, increasing almost 20 times in 2012 compared to 1992 (Jiang et. al, 2017).

Fouling and Scaling

Fouling is defined as the accumulation of undesirable formation of deposits on a surface. With respect to membranes, it can be defined as the accumulation of foreign materials from feed water on the active membrane surface (Penña et. al 2012). Eric et. al 2008 proposed a new definition of RO membrane fouling comprising internal and external phenomena. Where, external fouling is defined as surface fouling comprising of three stages that is scale formation, cake formation, biofilm formation and internal fouling as change in the membrane structure due to physical compaction or chemical degradation that alters solute and solvent transport. The types of foulants in RO membrane fouling can be categorized as: inorganic, where salt precipitations occur such as metal hydroxides and carbonates, organic that is natural organic matter (NOM) such as humic acid, colloidal that are suspended particles such as silica and biological such as bacteria and fungi (Kang et. al 2012). The fouling of membranes deteriorates the membrane functions such as salt passage

through the membrane, permeate flow, and pressure drop across the membrane (Valavala et. al 2011).

To avoid the issue of fouling and scaling it is necessary to have a pretreatment method to enhance the feasibility and efficiency of RO systems (Jamaly et. al, 2014). The pretreated feed water results in a lower undesirable fouling materials deposit on the membrane surface. The pretreatment methods can change the physiochemical and biological properties of feed water to improve the performance of RO units (Jiang et. al 2017).

Pretreatment technologies in RO systems

The pretreatment method can be selected based on the compositional analysis of the water source (Jiang et. al, 2017). In addition, comprehensive understanding of raw water quality and characteristics, and type of water resource is important to select appropriate pretreatment technology for RO system. For instance, membrane scaling can be reduced if the feed water with high hardness level can be pretreated to reduce hardness. Furthermore, with respect to the sources of water, surface waters have high turbidities, silt density index (SDI), and NOMS as compared to water from well sources. Identically, well water consist high silica content than surface water (Jamaly et. al, 2014). Therefore, pretreatment techniques can be targeted, altered and catered as per requirement. In general, conventional pretreatment includes acid addition, chlorination, coagulation/flocculation, disinfection, pH adjustment, scale inhibition, and media filtration and non-conventional technologies like UF and MF filtration.

Recently, a statistical analysis (Jiang et. al, 2017) revealed the common RO pretreatment technologies studied in the past 10 years were UF, coagulation/flocculation

and MF. So far, coagulation is the most popular pretreatment process and a successful method for improving the water quality not only in conventional pretreatment technologies, but also in low pressure membrane pretreatment technologies (Jamaly et. al, 2014). Coagulation is the process of destabilizing suspended solids, combine small particles into larger aggregates/floc by neutralizing the charges of the particle (Valavala et. al 2011). The colloidal matter and aqueous particulates are negatively charged and stay separated because of like charge repulsion. Thus, coagulants effectively neutralize like charges and allow suspended solids to group together in flocs. Typically, coagulants are small positively charged molecules (Lauren et al., 2009). Commonly, inorganic coagulants include ferric chloride or aluminum sulfate, while organic coagulants include low molecular weight (<500,000 Da) polymers (e.g., dimethyldiallylammonium chloride or polyamines) (Sweet water technologies, 2006; Lauren et. al, 2009).

Even though, the removal of colloidal and particulate matters is significantly enhanced, a study conducted by (Gabelich et. al, 2002) showed that coagulant residuals from pretreatment process negatively affects RO membrane performance when either aluminum/iron salts or chloramines were used. Overall, colloids and suspended particles passing through the conventional pretreatment frequently contribute to difficult to remove (and possibly irreversible) RO membrane fouling (Brehant et. al, 2008).

UF/MF Pretreatment Technologies

In the last two decades there has been a shift towards the use of larger pore size membranes (MF, UF and NF) to pretreat RO feed water (Pearce GK, 2007). These technologies have become widely accepted as a viable alternative to conventional pretreatment technologies like coagulation and settling (Cote et. al, 2001). The UF and MF membranes have seen an

increase in the number of installations and pilot-scale testing, however, pilot tests show successful implementation of NF pretreatment to RO systems as well. Both these modules have backwash cleaning and near dead end modes of operation that gives them an additional operational flexibility than the NF modules. According to research studies and pilot scale testing, UF are by far the most common choice (Brehant et al., 2003; Bu-Rashid and Czolkoss, 2007; Kamp et al., 2000; Pearce, 2007; Teuler et al., 1999; Tiwari et al., 2006; Vedavyasan, 2007; Wilf and Bartels, 2006; Xu et al., 2007) and have represented the best balance between contaminant removal and permeate production.

As discussed earlier, RO membrane can be easily polluted by accumulation of substances such as particles, biofilm and organic macromolecules. For certain situations discussed by Bonnelye et. al. (2008), the particle removal efficiency could reach 100% efficiency with UF and MF. Moreover, a constant quality feed water was achievable by UF with addition of a small amount of chemicals or no chemicals (Teng et. al, 2003; Zhang et. al., 2006a). Furthermore, Bae. et. al. (2011) found that the sum of relative abundance of biofilm-forming bacteria decreased by 90% by using non-conventional pretreatment as compared to 30% decrease by conventional pretreatment. Additionally, UF/MF pretreatment can be more economical for long-term operation that can be achieved by reducing energy consumption, use of chemicals, cleaning frequency and RO membrane replacement (Jiang et. al, 2017).

MF, UF or NF offers several advantages as a pretreatment to RO compared to conventional multi-media filtration. These membranes serve as a defined barrier between the RO system and any suspended particles. As reported by Tiwari et. al. (2006); Vedvyasan et. al (2007), membrane treatment can lower SDI to less than 2, and lower

turbidity to less than 0.05 NTU (Bartels et. al, 2006; Pearce, 2007; Xu et al., 2007). Also, they are advantageous to systems that treat surface water because they tend have more organic colloidal and suspended solids and sporadic problematic events such as algal blooms and chemical contamination (Lauren et. al, 2009). Overall, the potential benefits of membrane pretreatment over conventional pretreatment (Jamaly et. al, 2014) can be listed as : (a) lower suspended solids and less biological content,(b) lower RO pressure drops from fouling, resulting in lower energy costs,(c) longer RO membrane life, (d) increased flux rates in RO systems, (e) shorter plant footprint size resulting in reduced capital investment and, (f) lower chemical and sludge handling costs.

Although the membrane treatment process can significantly enhance the performance of RO membranes, the key disadvantage lies in the inherent propensity of a membrane to separate foulants from product water and, in the process, fouling itself (Lauren et. al, 2009). Both surface fouling and pore fouling are encountered in UF and MF membranes. The phenomenon of fouling prevents general operation at high permeate flux and, membrane damage and flux decline. Due to this, UF and MF membranes are typically replaced every 5-10 years (Pearce, 2007).

Hydrophilic Pretreatment Membranes

Fouling is often associated with hydrophobic surfaces because of the repulsion of water from their surface. Proteins, emulsified oils, microorganisms etc., have a high propensity for adhesion to hydrophobic membranes than hydrophilic membranes. This is a spontaneous process with increasing entropy, and the foulant molecules often tend to dominate the boundary layer and adhere to these surfaces. Whereas, studies show that

hydrophilic surfaces are less prone to fouling effect due to the decreased interaction between membrane surface and foulant (Hilal et. al, 2005; Fame and Fell, 1987; Nabe et. al 1997). Furthermore, there exists very low or no interaction of hydrogen bonds in the boundary layer between water and the membrane interface. Hydrophilic surfaces are hypothesized to tightly bind a layer of water that frustrates the deposition of foulants from the aqueous media (Miller et. al, 2017). Therefore, a modified membrane with hydrophilic character further enhances the formation of hydrogen bonds with water molecules thus preventing or reducing the adhesion of foulants on the membrane surface (Otitoju et. al 2018).

Introducing hydrophilicity to a hydrophobic membrane surface can thus aid the prevention of contact between the solute and the membrane surface mitigating the fouling effect. In the past hydrophilic modification has been achieved by blending, coating, surface grafting, surface physical treatments etc. This work aims at utilizing electrospinning technique to fabricate pretreatment membranes with tunable hydrophilicity. Furthermore, it is hypothesized that by controlling the ratio of a hydrophobic polymer and hydrophilic polymer during electrospinning, desirable membrane performance properties can be achieved like high solute rejection, foulant resistant and permeability.

Electrospinning

Electrospinning is a scalable and cost-effective technology which utilizes electrical forces to produce polymer fibers with diameter ranging from 2 nm to several micrometers using a polymer solution (Bhardwaj et. al, 2010). Furthermore, this technique offers several advantages of high surface area to volume ratio, tunable porosity and ability to get desired nanofiber properties and functions. Due to its versatility in spinning polymeric fibers and

their unique capabilities, electrospinning has been successfully applied in fields, such as, nanocatalysis, tissue engineering scaffolds, protective clothing, filtration, biomedical, pharmaceutical, optical electronics, biotechnology, healthcare, and environmental engineering, defense and (Bhardwaj et. al, 2010). A typical electrospinning setup consists of a high voltage power supply, a syringe pump holding the spinneret and a ground collector (usually a steel wire mesh, a metal plate or a rotary drum). Figure 2 shows typical setups of electrospinning apparatus that are commonly employed.

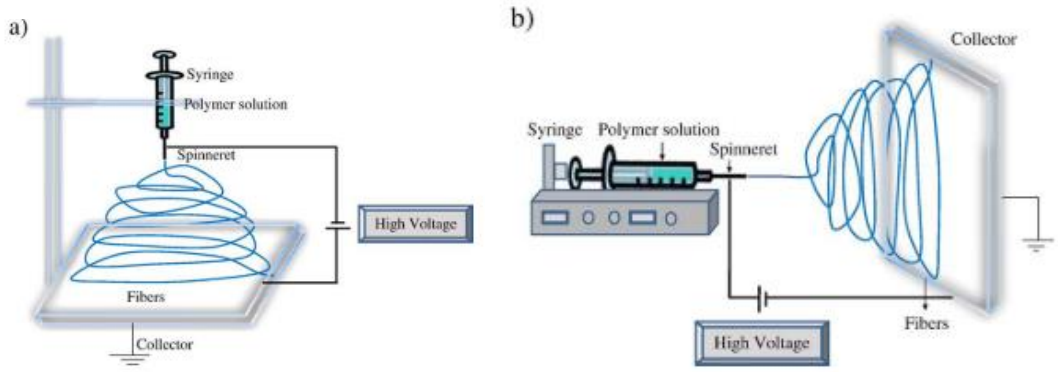

Figure 2. Typical electrospinning apparatus schematic (a) Vertical setup, (b) Horizontal setup (Bhardwaj et. al, 2010)

In electrospinning, a high electric potential is applied to a polymer solution. This is typically in the range of 5-30 kV that leads to charge injection into the liquid from the spinneret. The charged liquid is then attracted to the ground electrode kept at a distance away, forming a so-called Taylor cone at the nozzle orifice (Yao et. al, 2003). The polymer solution from the nozzle orifice is drawn out by the electric field to form a liquid jet. As the liquid jet runs towards the electrode, the solvent evaporates, and the jet solidifies depositing on the ground collector as fibers. Furthermore, the electrospinning parameters

such as, applied voltage, flow rate and tip to collector distance can be tailored yielding different nanofiber morphologies as desired. Therefore, the aim of fabricating tunable hydrophilic pretreatment membranes can be achieved by employing electrospinning process effectively.

Poly(vinyl chloride) (PVC) is a hydrophobic polymer widely used in water treatment technology as a UF/MF membrane (Zhang et. al, 2009; Dong et. al, 2013). PVC possess outstanding mechanical properties, resistant to a variety of acids, bases and organic compounds. Due to its mechanical properties, PVC provides support and stability to ensure membrane durability at high pressure drops. However, the hydrophobicity of PVC membranes makes them vulnerable to fouling, wherein, colloids, NOM, and microorganisms tend to deposit on the membrane surface during filtration process (Hong et.al, 2018). This deposition of foulants on the surface often causes decrease in water flux, increased frequency of backwashing and membrane maintenance cost. Therefore, introducing hydrophilicity to these membranes can mitigate the effects of fouling.

Poly(vinyl alcohol) PVA is water soluble polymers that has garnered attention due to its low cost, high hydrophilicity and excellent chemical resistant (Quinn et. al, 2018). Moreover, PVA's biocompatibility has enabled its application is tissue engineering, biocompatible glucose sensing and hydrophilic modifiers to promote water flux and antifouling performance for water treatment (Ren et. al, 2006; Kang et. al, 2011). Furthermore, PVA is amenable to several post-processing chemical reactions like functionalizing with selective ligands. Therefore, PVA and PVC polymeric solutions were dual electrospun to fabricate pretreatment membranes with tunable hydrophilicity.

For this work, electrospun membranes were prepared at increasing mass flow ratios of PVA/PVC, while holding PVC constant to study the effect of membrane hydrophilicity. Dual electrospinning technique i.e. simultaneous deposition of two polymer solutions to create a co-spun mat is explored and a rigorous analysis method will be developed to map the concentration of each polymer on the membrane surface. In addition to this, membrane characterization techniques will be performed to confirm the presence of both polymers. PVA in the co-spun mats will be crosslinked to impart mechanical strength and make them compatible for filtration studies. Furthermore, this work aims to establish a correlation between the mass flow and the mass deposition ratio in order to accurately study the effects of PVA concentrations on the membrane's hydrophilicity. Additionally, it is expected that increasing the PVA content on the co-spun mats would result in better filtration conditions and have higher flux values. Lastly, it is hypothesized that increased PVA content would have a positive correlation with the tensile strength of these fabricated co-spun mats.

CHAPTER 2

MATERIAL AND METHODS

Solution Preparation

For the dual electrospinning, polymer solutions of PVA and PVC were prepared separately. Poly(vinyl alcohol) (PVA, M_w = 89,000-98,000, 99%+ hydrolyzed) and Poly(vinyl chloride) (PVC, Mw = 80,000) was purchased from Sigma-Aldrich. N, N-dimethylformamide (DMF, ≥99.8%), Tetrahydrofuran (THF) and Triton X-100™ were purchased from Sigma-Aldrich. Ultrapure water was dispensed from Milli-Q® water purification system. A 12% PVA solution was prepared by adding PVA powder to room temperature ultrapure water. This solution was continuously stirred for approximately 30 mins at 500 rpm to ensure the hydration of PVA in the solution (Quinn, et. al, 2018). The solution was then kept in an oil bath at 90°C for 30 mins at 500 rpm to fully dissolve. It is important to let the solution temperature reach 90°C to obtain a clear homogenous solution. It is recommended to use an oil bath for solution preparation instead of hot plate to ensure the solution reaches the desired temperature. For PVC, a 15% PVC solution was prepared by dissolving PVC powder in a mixture of 1:1 ratio (wt. %) of DMF and THF solvents. The solution was stirred at 500 rpm for 6 hours at 60°C to let PVC fully dissolve in the solvents. After dissolution, both polymer solutions were kept under constant stirring.

Crosslinking reaction

PVA mats were crosslinked by submerging the prepared mats in a solution of poly(ethylene glycol) bis(carboxymethyl) ethyl (Sigma , Mn = 600 g/mol) or polyethylene glycol 600 diacid (PEGDA) and methanol (MeOH, Sigma, ≥99.8%). To this solution, a drop of hydrochloric acid (HCl, Fisher, 36-38%) was added to catalyze the reaction and ensure the completion of crosslinking reaction. 0.005 g of PVA nanofibers were immersed in a 20 ml 0.1 M PEGDA – MeOH with one drop of HCl. The PEGDA-MeOH concentration was varied from 0.1 M to 0.0075 M to study the effect of concentration of crosslinker on the PVA mats. Before immersing the PVA mats, the solution was stirred for 5 mins to unsure complete mixing. The submerged mats were heated to 80°C for 30 mins in the oven. After the crosslinking reaction, PVA mats were washed with DI water to ensure removal of solution from the surface of the membrane. The mats were then kept under atmospheric conditions for 24 hours to dry.

CHAPTER 3

EXPERIMENTAL METHODS

Electrospinning of PVA

To optimize the electrospinning conditions, a 2^3 full factorial design of experiment study was performed with 12% and 15% PVA solutions. The full factorial study was evaluated with flow rate (F) (0.75 and 1.5 ml/hr.), applied voltage (V) (18 and 23 kV) and tip-to-collector distance (T/C) (12 cm and 15 cm). The aqueous solutions of fully hydrolyzed PVA under lab conditions and without any additive do not electrospun efficiently; wherein the solution accumulates on the tip of the syringe and sporadically electrosprays as droplets on the collection foil. Therefore, PVA electrospinning was stabilized by adding Triton X-100™ surfactant (0.58 w/w %). In addition to this, PVA syringe was fitted with a 3 - way adapter spinneret for gas (air) (0-30 psi) assisted electrospinning in the modified dual electrospinning setup.

Electrospinning of PVC

A solvent ratio of 1:1 of THF: DMF was chosen for PVA based on fiber morphology analysis from initial sets of experiments. Like PVA solutions, a 2^3 full factorial design of experiment study was conducted for 15% PVC solution. The test conditions for 2 level 3 factor study included flowrate (F) (0.5 and 1 ml/hr.), applied voltage (V) (12 and 18 kV) and tip-to-collector distance (T/C) (12 and 15 cm).

Dual Electrospinning

Due to a lack of common solubility of both polymers in a solvent, a rotary drum collector was used to simultaneously deposit the nanofibers of PVA and PVC. The drum was covered with an aluminum foil to facilitate the replacement after each spin. An aluminum can was used as the drum and rotated at 10 RPM throughout the experiment. KD scientific syringe pumps were used to meter the PVA and PVC solutions, and a CZE1000R Spellman and Gamma high voltage research ES30P-5W HV power supply were used to produce the applied voltage. Figure 3 shows the schematic of the dual electrospinning used for fabricating co-spun mats.

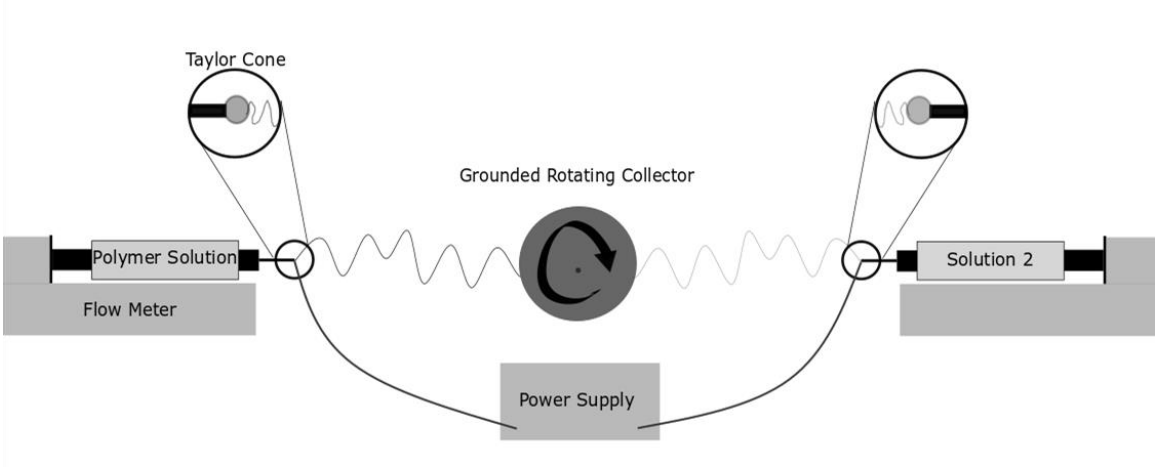

Figure 3. Schematic of dual electrospinning setup with a rotary collected utilized to simultaneously deposit two distinct polymer solutions.

Membrane Characterization:

Scanning electron microscopy (SEM) imaging was done on AMRAY 1910 Field Emission SEM operating at 15 kV to characterize the fiber diameter, membrane thickness and morphology. The nanofiber samples were sputter coated with gold particles before imaging

and analyzed at various magnification. Fiber diameter and pore size measurements were analyzed using open source ImageJ software. In addition, the EDAX detector on the SEM was used to perform energy dispersive x-ray analysis (EDX) for elemental analysis on the nanofiber sample. Confocal fluorescence microscopy was taken on a Nikon C2 laser scanning confocal on a Nikon Ti inverted microscope base. The dye was excited with a 488 nm laser and emission detected at 575-625 nm. Images were collected with a 60X oil immersion lens with numerical aperture of 1.4. The differential interference contrast image was made simultaneously using the transmitted light from the 488 nm laser. Additionally, Fourier transform (FTIR) spectra (4000-400 cm^{-1}) were obtained on a Nicolet™ iS™ spectrometer at 4 cm^{-1}resolution and 32 scans.

Membrane Filtration

The prepared co-spun crosslinked membranes were subjected to filtration experiments using a 300 mL Sterlitech HP4750 stirred, dead end filtration cell with an effective area of 14.6 cm^2. Sartorious ED3202S extend precision balance connected with a LabVIEW software was used to measure the flowrate every 3 s. All the membrane mats were supported with two layers of filter paper and filtration experiments were performed at room temperature. The filtration tests were recorded under a 5.7 psi pressure. Flux (Lm^{-2} h^{-1}/psi or LMH/psi) calculations were done by measuring the flow rate through the membrane normalized by the membrane active area.

Tensile Test

The durability and mechanical strength of the crosslinked co-spun membranes was investigated using tensile tests on the TA instruments DHR-2 in tensile mode. The membranes were tested at a constant crosshead speed of 10 µm/s at 23 °C.

CHAPTER 4

RESULTS AND DISCUSSION

Prior to dual electrospinning of PVA and PVC solution, each of these solutions were electrospun separately to optimize the electrospinning parameters and study the effect of these parameters on fiber diameter and morphologies. Tarus et. al (2016) studied the effect of solution concentration on fiber diameter for the PVC polymer. At lower concentrations, there is a tendency for PVC solution to form beaded fibers and an increase in the fiber diameter is observed with increased concentration attributed to the changes in viscosity. The increase in viscosity with higher solution concentration is related to increase in polymer chain entanglement due to increase in the numbers of polymer molecules. Furthermore, this increase in the polymer chain entanglement enables solvent molecules to distribute over entangled polymer molecules directing them to form smooth fibers and improved fiber uniformity (Mit-uppatham et. al, 2004). Tarus et. al 2016 were able to obtain smooth and uniform fibers at 14% and 16% PVC prepared in DMF/THF 1:1 (w/w) system. Therefore, a 15% PVC solution was chosen with the same solvent system.

A 2^3 full factorial study was performed to identify the most significant factor affecting the fiber diameter and morphology for the 15% PVC solution. Electrospun PVC mats were examined under SEM and fiber diameter calculations was done by choosing 100 fibers at random. After analyzing the data with six sigma tools, the pareto plot were generated (appendix A2.3) that showed no significant factor affecting the fiber diameter with the chosen highs and lows for flow rate, applied voltage and tip-to-collector distance. The average fiber diameter (FD) (Table A2.1) ranged from 264 ± 127 nm to 468 ± 264 nm for the given electrospinning parameters. Additionally, fiber morphologies were compared

for the 8 runs (appendix A) and based on the least standard deviation the electrospinning parameters were chosen for the dual electrospinning. From the SEM images, it was observed that the PVC mat were comprised of stiff and rigid fibers.

Similarly, a 2^3 full factorial design study was performed for the electrospinning of PVA polymer. Aqueous solutions of 12% and 15% PVA were electrospun at varying conditions to get average fiber diameter data. Jeffery et. al. (2017), from the group previously demonstrated a study on PVA nanofibrous membranes with a 9% PVA solution, however, a higher concentration of PVA was chosen for this study to introduce more hydrophilic character to the dual spun mats. While electrospinning of 12% and 15% solutions, it was observed that with the 15% PVA solution, a uniform Taylor cone and a stable jet could not be achieved with the given sets of parameters. Moreover, the PVA solution would accumulate on the tip of the needle and would periodically electrospray as big blobs on the rotary drum. The electrospinning conditions did not stabilize even when the flow rates and applied voltage were varied in capacity. Similar observations were recorded with the 12% PVA solution, however, the frequency of instability in the Taylor cone was far less than the 15% PVA solution and thus was chosen for further electrospinning experiments.

The phenomena of instability in the jet can be understood by Taylor's theory for the case of PVA. During electrospinning process, a droplet of polymer solution is deformed into a conical shape, known as the Taylor cone, from which the polymer jet erupts. Additionally, Taylor, G., (1969) established that the critical electric voltage of formation in the Taylor cone is proportional to the surface tension of the solution. Furthermore, Finch, C. A, 1973 suggested that the surface tension of aqueous PVA solutions has dependence

on the degree of hydrolysis of PVA. The surface tension would become more pronounced when the degree of hydrolysis approached 100%. In this case, either PVA solutions would require a higher voltage to initiate the Taylor cone or decrease in surface tension to produce uniform fiber jets.

Table A1, in the appendix A, shows the average fiber diameter and their standard deviation from the 2^3 full factorial design experiments for PVA. The electrospun 12% PVA mats consisted of average fiber diameters ranging from 148 ± 34 nm and 182 ± 41 nm. In comparison to the PVC fibers that look strong and rigid from scanning electron micrographs in Figure 4, PVA fibers appeared fluid and less rigid. Similarly, for PVA, there were no significant factors (Appendix A1.3) that affected the average fiber diameter, however, based on the evaluated fiber diameter data and membrane morphology electrospinning conditions were determined for dual spinning.

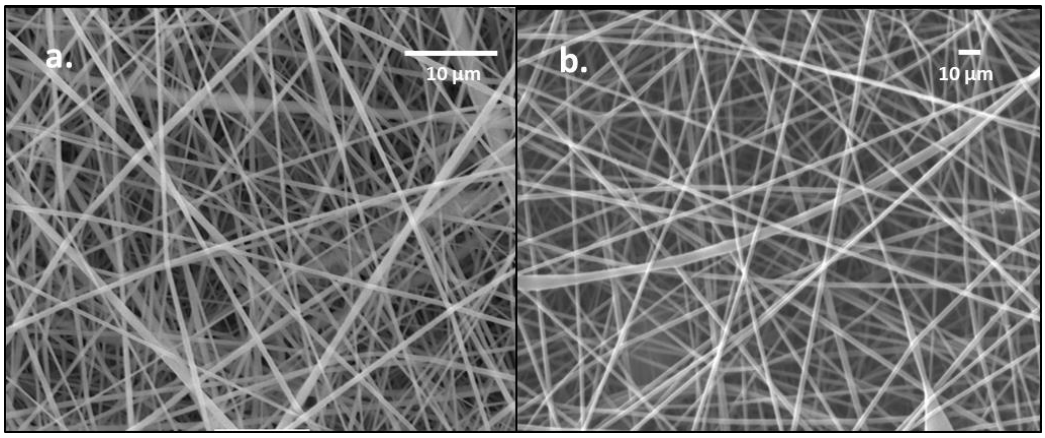

Figure 4. Scanning electron micrographs for (a) 15% PVC fibers, (b) 12% PVA fibers

As discussed above, the variations in the fiber morphology of as-spun PVA fibers is due to the high surface tension that disables smooth electrospinning conditions. To facilitate and enhance the electrospinning of 99.5+% hydrolyzed PVA, Triton X-100™ surfactant was added to lower the high surface tension of the of the PVA solutions. On

addition of a small quantity of Triton X-100™, a fine stable jet of polymer was ejected from the polymer droplet at the nozzle orifice. Moreover, continuous fibers were deposited without breakage of the Taylor cone and jet, forming a non-woven fibrous mat on the rotary drum. It was also observed that the PVA jet further stabilized by applying high voltage of 22-24 kV.

Dual Electrospinning

After examination of the electrospinning conditions and estimating their average fiber diameters, it was possible to analyze the characteristic of a co-spun mat (used interchangeably with membrane) with PVA and PVC and attribute it to either one of them or both the polymers. For the dual electrospinning, 15% PVC solution was electrospun at 1 ml/hr, 12kV and distance of 12 cm, and 12 % PVA-TX (with Triton X-100™) solution at 0.75 ml/hr, 23 kV and 12 cm. After completing the simultaneous deposition of both polymers on the same mat, samples of the co-spun mat were observed under the SEM. Figure 5 shows scanning electron micrographs with the statistical distribution of fiber diameters for control samples of 12% PVA-TX, 15% PVC and the co-spun mats. In addition, Table 1 shows the average fiber diameter (FD) for the co-spun mat is 245 ± 106 nm that lies between the fiber diameter of the two as-spun control samples. Moreover, by examining the SEM image of the co-spun mat, it appears to be a mixture of both PVA and PVC, exhibiting their defining characteristics and suggesting the presence of both PVA and PVC.

From the statistical analysis of the fiber distribution, the co-spun mat shows that most of the fibers have diameter greater than 200 nm characteristic to that of PVC fibers. When comparing the fiber distribution of co-spun vs PVA mat, it is evident that the

contribution of PVA in the co-spun mat is less or absent. Moreover, the PVC and co-spun diameter distribution is quite similar suggesting that this quantitative analysis is not enough to conclude the existence of both the polymers on the co-spun mat. Therefore, complementary analytical techniques must be used to determine if PVC and PVA have been successfully deposited onto the same mat.

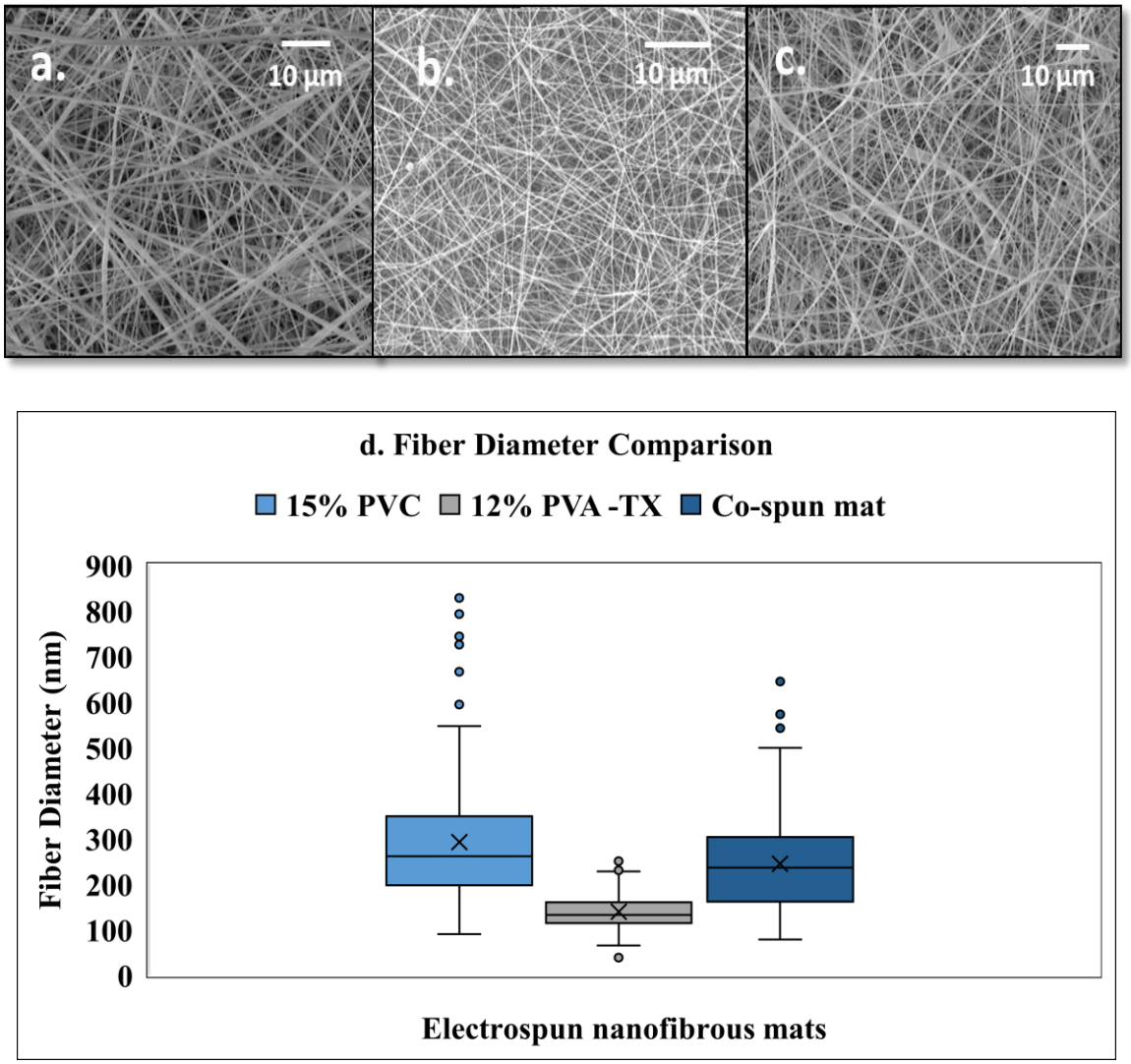

Figure 5: Scanning electron micrographs of (a) 15% PVC, (b) 12% PVA –TX, (c) Co-spun mat and (d) fiber diameter comparison of the 3 electrospun mats.

Table 1. Electrospinning parameter and average fiber diameter data collected from control samples of PVA, PVC and co-spun mats from 100 random fibers.

Polymer	F(ml/hr)	T/C (cm)	V (kV)	FD (nm)
15 % PVC	1	12	12	293 ± 132
12% PVA -TX	0.75	12	23	150 ± 38
Co-spun				245 ± 106

Energy dispersive X-ray spectroscopy (EDS)

A complimentary technique to SEM, Energy dispersive X-ray spectroscopy or EDS, is an analytical technique used for elemental analysis or chemical characterization can be used to confirm and quantitatively estimate the relative concentration of PVA and PVC. EDS are generally performed in conjunction with SEM and is a standard method for quantifying and identifying elemental compositions in a small sample. The EDS technique captures the X-rays using a detector that are emitted from the sample after bombardment of electrons in an analyzed volume often ranging from micro- to nanoscale.

The characterization capabilities of this technique rely on the fundamental principle that each element has a unique atomic structure that allows it to exhibit a unique set of peaks in its X-ray spectrum. In EDS technique, the electron beam is focused in the region of interest in the sample to stimulate the emission of characteristic X-rays. More importantly, the generation of X-rays is a two-step process. The first step is associated with the transfer of energy to the atoms when the electron beam hits the sample. This energy can be utilized by the electrons of atoms to jump to an energy shell with higher energy or get knocked off from the atom. Moreover, with such a transition the electrons leave behind

a hole, that are associated with a positive charge. In the second step, the generated holes attract electrons from a higher energy shell. When an electron from such a higher energy shell fills the hole of the lower-energy shell, the energy difference associated with the transition is released in the form of an x-ray energy. As mentioned above, the x-ray energy is characteristic of the element from which it was emitted.

By acquiring the data for energies of the X-rays emitted from the region of interest being excited by the electron beam, the elements in the sample can be determined. Therefore, the acquired spectra show a qualitative analysis of the types of elements in the sample. Additionally, the rate of detection of these X-rays can be used to measure the amount of the elements in the sample. By measuring the number of counts collected of each peak in the spectra, the EDS can be utilized to make a quantitative analysis. Furthermore, by operating the EDS in quantitative mode, the X-ray maps can be acquired showing the spatial variation of the elements in the sample.

The co-spun mat fabricated from dual electrospinning were analyzed by the EDS technique. A total of 15 locations were chosen covering the entire surface area of the mat. The electron beam was set to a gun voltage of 20kV compared to 15 kV for SEM to generate high number of electrons from the sample. Before loading the sample, the co-spun mats were placed on the stubs and sputter coated with gold (Au) particles. In addition to this, the co-spun mat was electrospun on an aluminum foil (Al) paper, therefore, the collected spectra obtained from the sample had peaks of Au and Al. Since, the amount of coated Au layer and foil sample size was same for each sample, the counts for both were removed while quantifying the peaks. Also, any peak other than carbon (C), oxygen (O) and chlorine (Cl) were removed to help in the analysis and quantification. Figure 6 shows

the elemental map generated from collecting the average composition of C, O and Cl for the co-spun mat.

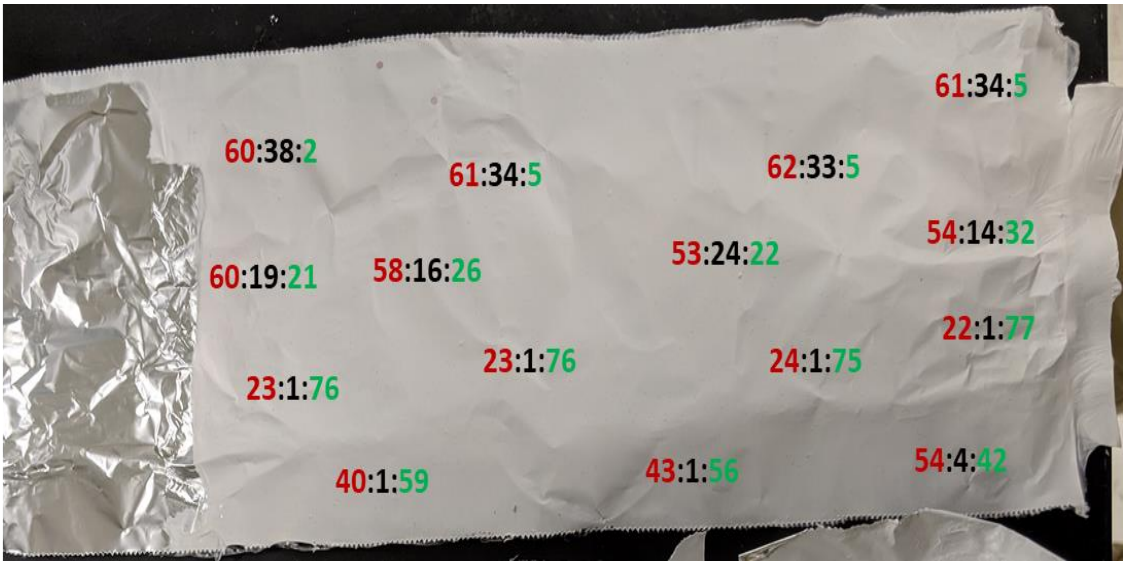

Figure 6: Elemental map collected from 15 locations in a co-spun mat containing PVA and PVC, where **carbon (-C)** is represented by **red**, **oxygen (-O)** by **black** and **chlorine (-Cl)** by **green**. The data mapped gives the weight percent composition in the format **(C:O:Cl)**.

To confirm the presence of both polymers on the co-spun, PVA and PVC were identified with O and Cl, respectively. In addition to O and Cl peaks, C peak was recorded to report the elemental data of the two functional groups with respect to carbon. In the above Figure 6, the reported data is given in weight percent (wt. %) calculated based on the C, O and Cl peaks from the EDAX Genesis software.

The EDS analysis confirms the presence of PVA and PVC on the co-spun mat. Looking at the elemental map the corresponding peaks of O and Cl were detected throughout the entire mat. This finding affirms the successful deposition of PVA and PVC onto the same mat. On further analysis, it appears that the concentration of O and Cl are

not uniform across the membrane mat. The upper section displays a higher concentration of O indicating accumulation of PVA fibers, while the lower section has a higher concentration of Cl suggesting accumulation of PVC fibers. Moreover, the central section of the membrane shows a more uniform fiber distribution of both the polymers with respect to each other (Figure 7). This data analysis suggests that during the dual electrospinning there is partial deposition of both polymers on either side of the mat.

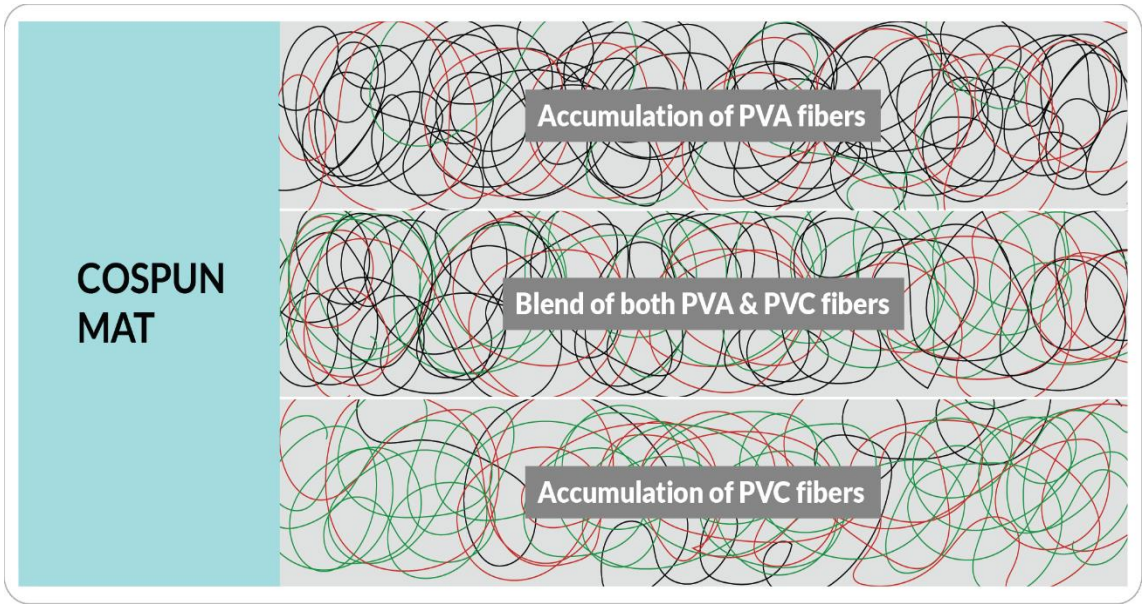

Figure 7: Illustration of partial deposition of PVA and PVC fibers across the membrane surface from EDS technique. PVA fibers are represented as black and PVC fibers as green, while the red fibers are only included for showing the presence of carbon in the co-spun mat based on EDS data analysis.

The difference in relative concentration can be associated to the limitations of the dual electrospinning setup. With the current setup, each side of the mat is dominated by a specific polymer, whereas, only the central section has uniform deposition of both

polymers. While the data shows there is inconsistency in the deposition and spatial variation in the elements, the presence of both PVA and PVC is clearly detected. This analysis further implies that there is a need to identify an experimental setup that can provide consistent deposition of PVA and PVC. Later section of this chapter discusses a suggested modification in the electrospinning setup to address the issue of this partial deposition.

Fourier Transform Infrared Spectroscopy (FTIR)

Besides EDS technique, another complementary analytical technique was performed to affirm the deposition of both polymers. Fourier transform infrared spectroscopy (FTIR) was used to obtain the infrared spectrum of absorption of 12% PVA-TX, 15% PVC and the co-spun mats. FTIR spectroscopy shows several absorption peaks that can be used to investigate the presence of functional groups in the sample. Moreover, the different bond vibrations present in a sample can be analyzed using the FTIR spectroscopy. To identify and confirm the peaks in the co-spun mat, its FTIR spectra was compared to that of 12% PVA-TX and 15% PVC shown in Figure 8.

In the 12% PVA-TX FTIR spectra represented in blue, the peak between 3200 – 3550 cm^{-1} is a strong and broad peak and corresponds to the O-H stretching of the alcohol group in the poly(vinyl alcohol). This was chosen as the characteristic peak to identify PVA while examining the co-spun mat. For the case of 15% PVC (represented in red), the peaks between 650 – 810 cm^{-1} corresponds to characteristic C-Cl stretching in the fingerprint region and was used to identify the PVC. The CH_2-rocking vibration at 960 cm^{-1} in the 15% PVC samples was identified as another peak for comparison.

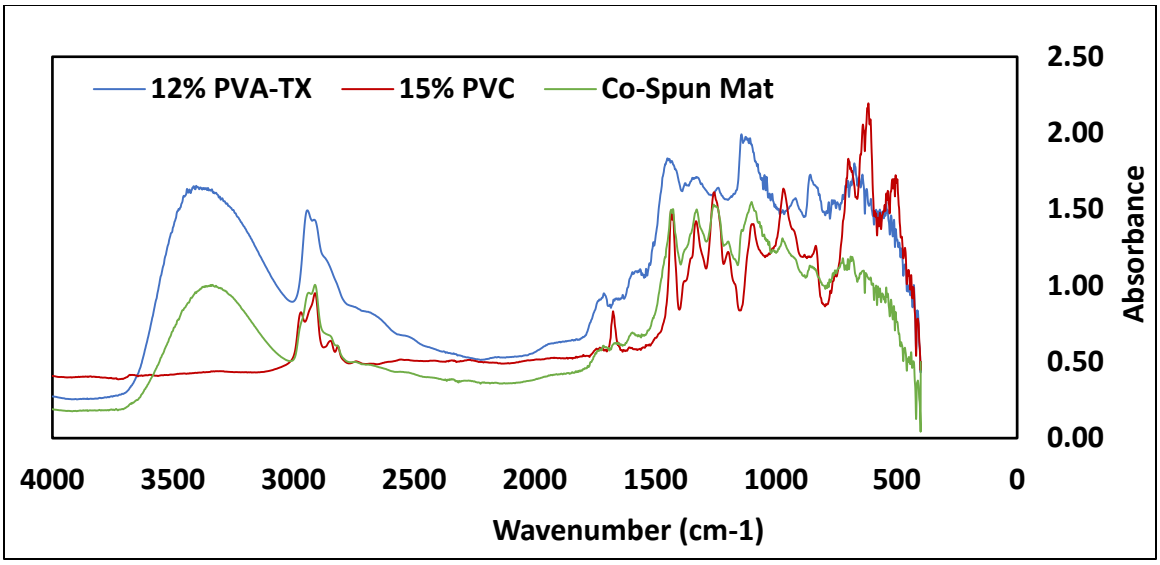

Figure 8. FTIR absorption spectra for 12% PVA-TX, 15% PVC and co-spun mat.

In Figure 8, the co-spun mat spectra showed both the characteristic peaks of C-Cl and -OH stretches. The C-Cl stretch is present in the co-spun mats (represented in green) and the peaks appear between 641 and 708 cm^{-1}. Although it is difficult to observe these peaks in the fingerprint region, on close observation the peaks are visible. Moreover, the CH_2 rocking vibration characteristic to PVC appears at 970 cm^{-1} which is absent in the PVA sample. At higher wavenumbers, the peaks corresponding to 1430 cm^{-1} is for the CH_2 bending and is common to both the PVC and PVA. Lastly, the -OH characteristic stretch was observed as a large band in the co-spun mat between 3200 – 3550 cm^{-1} indicating the presence of PVA. Thus, FTIR analysis of the co-spun sample, confirms the presence of PVA and PVC validating the qualitative results obtained from the EDS technique.

Confocal Fluorescence Microscopy

Confocal microscopy, an optical imaging technique that uses fluorescence optics was explored to trace the only the PVA on the co-spun mat. This optical microscopy technique was chosen because of its ability to control depth of field and eliminate or reduce the background information away from the focal plane. For this technique, the 12% PVA-TX solution was stained with Oil Red O (ORO) and electrospun with 15% PVC on the dual electrospinning apparatus to make a co-spun mat. The PVA on the co-spun mat were referred to as the labeled fibers, while the PVC fibers referred as unlabeled fibers.

In order to detect the ORO stain in PVA fibers, the confocal microscopy was performed using a 540 to 580 nm tetramethylrhodamine (TRITC) excitation/emission filter. Additionally, the transmitted light channel (TD) detector was also utilized to provide images for spatial registration with the fluorescence images. More importantly, the PVA solution were stained with an excess of ORO to help them identify from the unlabeled fibers and avoid autofluorescence from both sets of fibers. The optical images were then taken from the top surface and a layer below into the membrane.

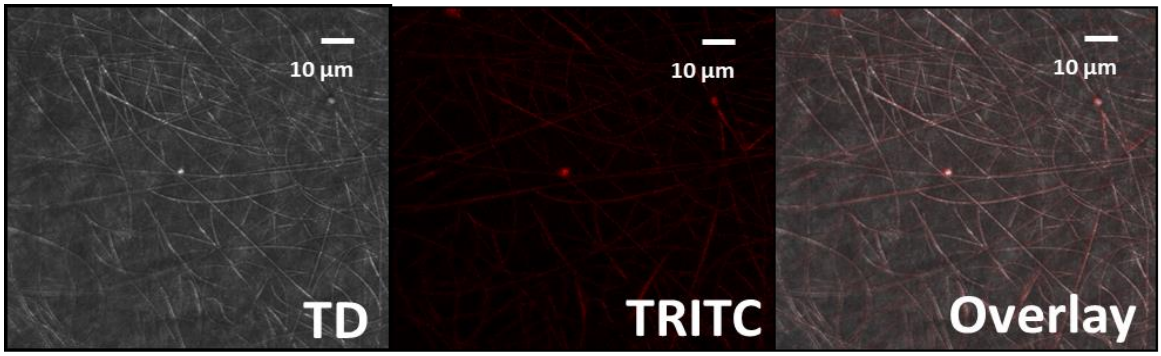

Figure 9a. Transmitted light (TD), red channel (TRITC) and overlay images for labeled fifibers at the top surface of the membrane.

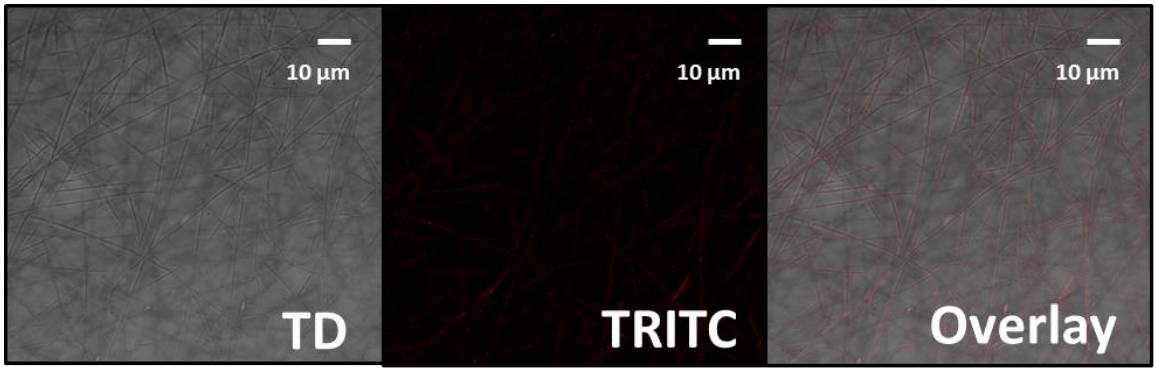

Figure 9b. Transmitted light (TD), red channel (TRITC) and overlay images for labeled fibers at the lower surface of the membrane.

Figure 9a and 9b shows the images from the transmitted light channel, red channel and the overlay of the two channels for each image from the top and the bottom surface. The overlay images seen in Figure 9a and 9b for both the channels at two separate locations are in registration to each other i.e. the fluorescence in the red channel confirms the real signal obtained from the labeled sample.

Furthermore, in order to confirm the presence of PVA fibers deeper into the membrane and to affirm that the fluorescence or the excitation/ emission light penetrates

through the sample, a pseudo-colored image was generated. In the pseudo-colored image (Figure 10), the different colors represent different imaging length in the same field. It was seen from the overlay in confocal of layers pseudo-colored differently that different PVA fibers at different layers in the sample were detected. Therefore, the set of labelled fibers were distinguished from unlabeled fibers at various depths of the membrane surface further corroborating the results obtained from all the above-mentioned analytical techniques.

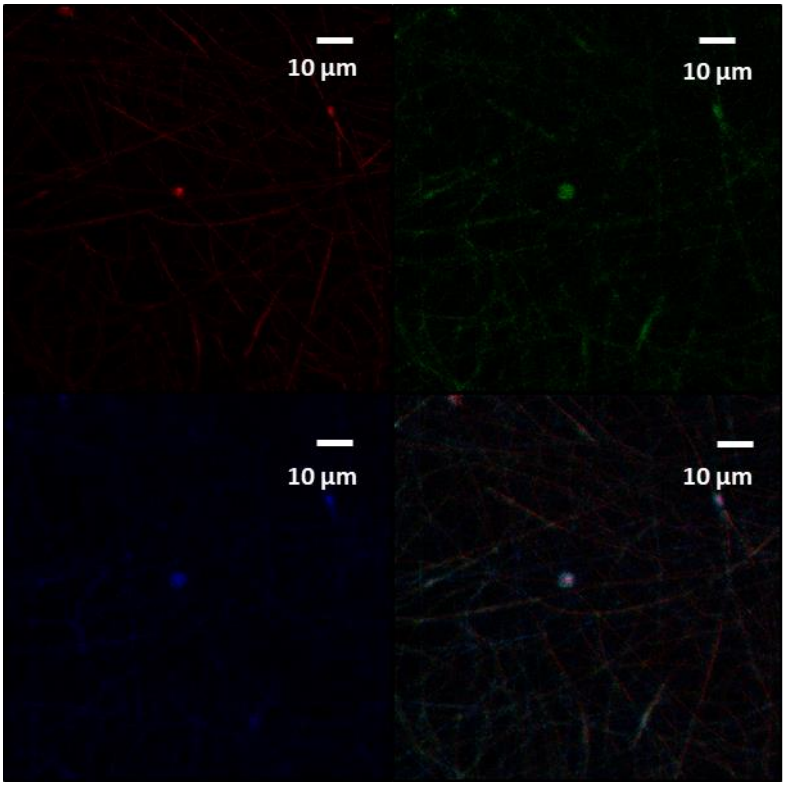

Figure 10. Pseudo-colored image of 3 different deep layers in the membrane imaged in the red channel (TRITC)

Crosslinking Reaction

The as-spun PVA nanofibrous mat possesses little or no mechanical integrity. More importantly, when they are immersed in water, the PVA mat completely shrinks and becomes a gelatinous material. For filtration conditions, it becomes important to crosslink the PVA fibers to impart mechanical strength. Furthermore, the as-spun fibers appear white because of light scattering from fibrous structure whereas, after immersion in water it becomes completely clear. Quinn et. al (2018) from the group studied crosslinking of PVA nanofibers using poly(ethylene glycol) diacids in isopropyl alcohol solution. This study utilized a short chain length and a long chain length PEGDA as a crosslinker and evaluated their effect on fiber characteristics. The PEGDA with 600 g/mol was found to create inter- and intra-fiber crosslinking and significantly increasing the tensile strength of the PVA nanofibrous mat.

In this work, the crosslinking reaction (Figure 11) with PEGDA-600 is further explored with a different solvent in order make the PVA nanofibers compatible for filtration experiments. The effect of crosslinking reaction was initially studied on PVA mats only before implementing them on the co-spun mats.

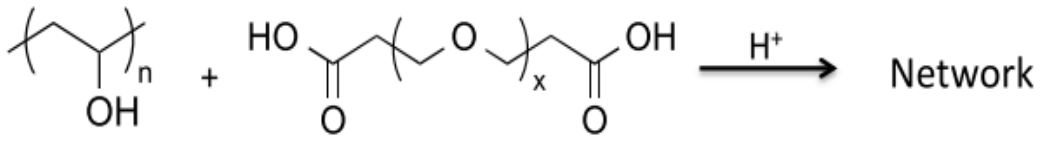

Figure 11. Chemical crosslinking of electrospun PVA mats using varying concentrations of PEGDA in methanol solution (PEGDA-MeOH).

The prepared electrospun mats were submerged in the 0.1 M PEGDA – MeOH solution at 80° C for the crosslinking reaction. Just by physical examination it can be estimated that PVA mats are crosslinked. When the nanofibers are collected, they often do not peel off easily and in some cases get stuck to the collector. On crosslinking, the PVA mat turn translucent and can be peeled off easily. Additionally, the surface appears smooth indicating the fibers have fused and integrated to form a rigid membrane. Moreover, it was found that after treating with PEGDA-MeOH solution, the integrity of the PVA is preserved after immersing in water.

On further analysis with the SEM revealed that the fibrous morphology of the PVA mats had retained the fibrous structure and the fibers had infused creating a smooth morphology on the surface of the membrane. As well as, from the scanning electron micrographs it was seen that the crosslinking reaction created pore cavities ranging from 0.5 – 1 μm between the fused PVA membranes seen in Figure 12.

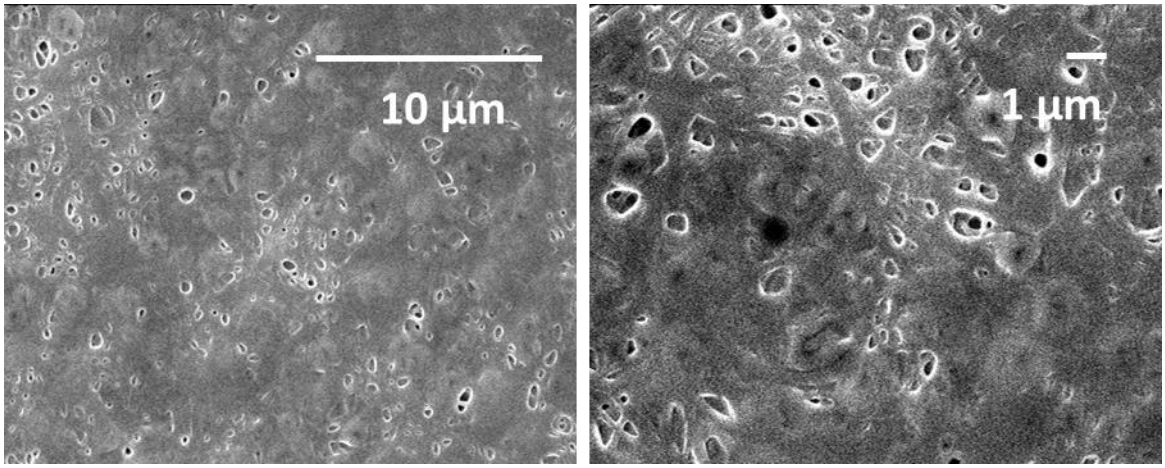

Figure 12. Scanning electron micrographs of the crosslinked PVA mats with 0.1 M PEGDA – MeOH solution at 10 μm and 1 μm scale.

In order to completely understand the crosslinking reaction, the effects of several factors like the crosslinking time, crosslinking temperature and the crosslinker strength were investigated. By varying the time from 5 – 60 mins and temperature from 80°- 90°C yielded the same results. Interestingly, it was found that on lowering the concentration of the PEGDA – MeOH concentrations from 0.1 M to 0.0075 M, the surface morphology of the PVA mats improved significantly. Figure 13 shows the improvement in the surface morphologies observed under SEM with 6 different concentrations of PEGDA – MeOH solutions. Consequently, it was observed that not only the surface morphologies improved but the average pore size between the fibers reduced drastically. The average pore size reduced approximately from 500 nm to 80 nm with decrease in the crosslinker strength shown in Figure 14.

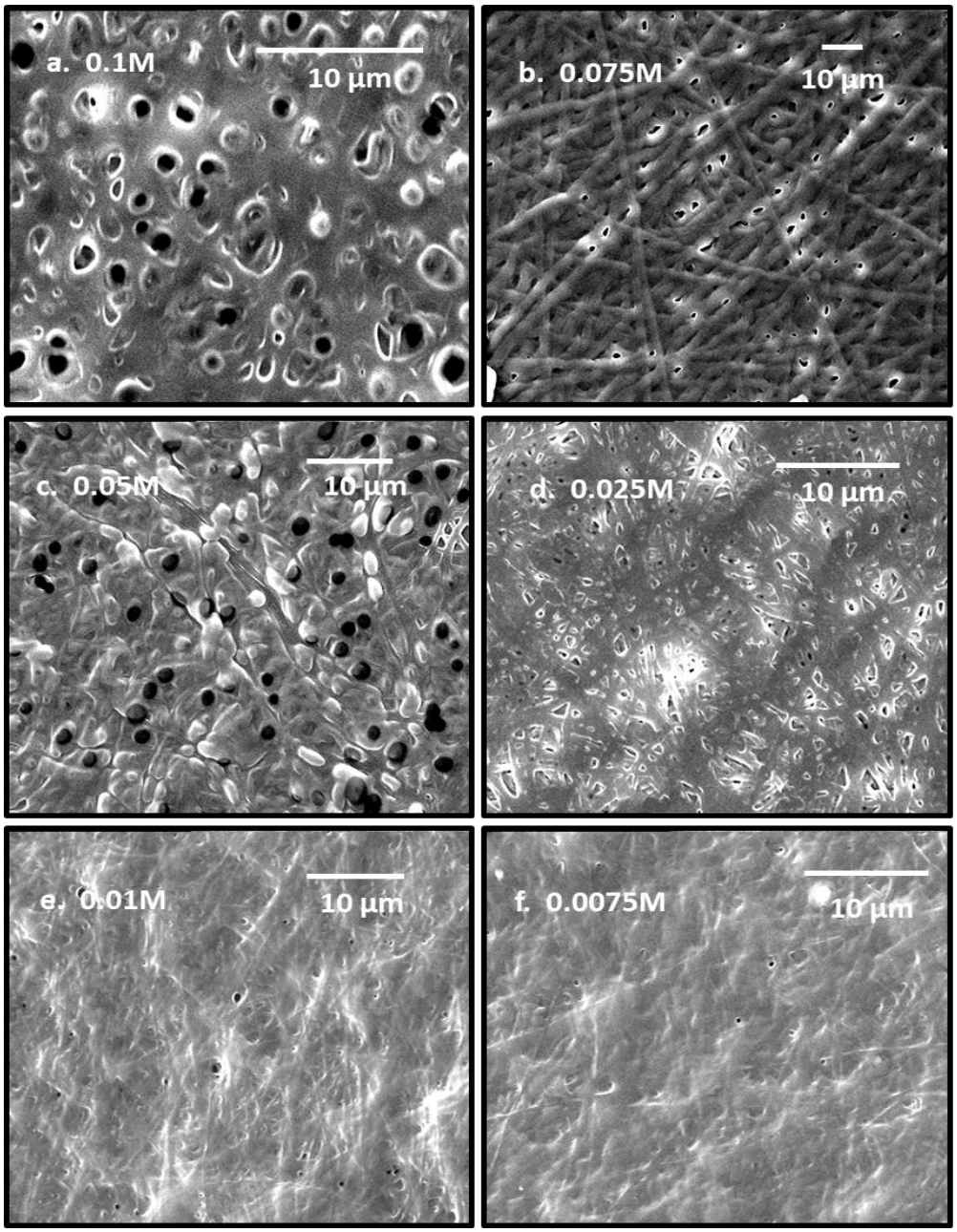

Figure 13. Scanning electron micrographs of crosslinked PVA with various crosslinker concentration showing improvement in surface morphology and reduction in pore size.

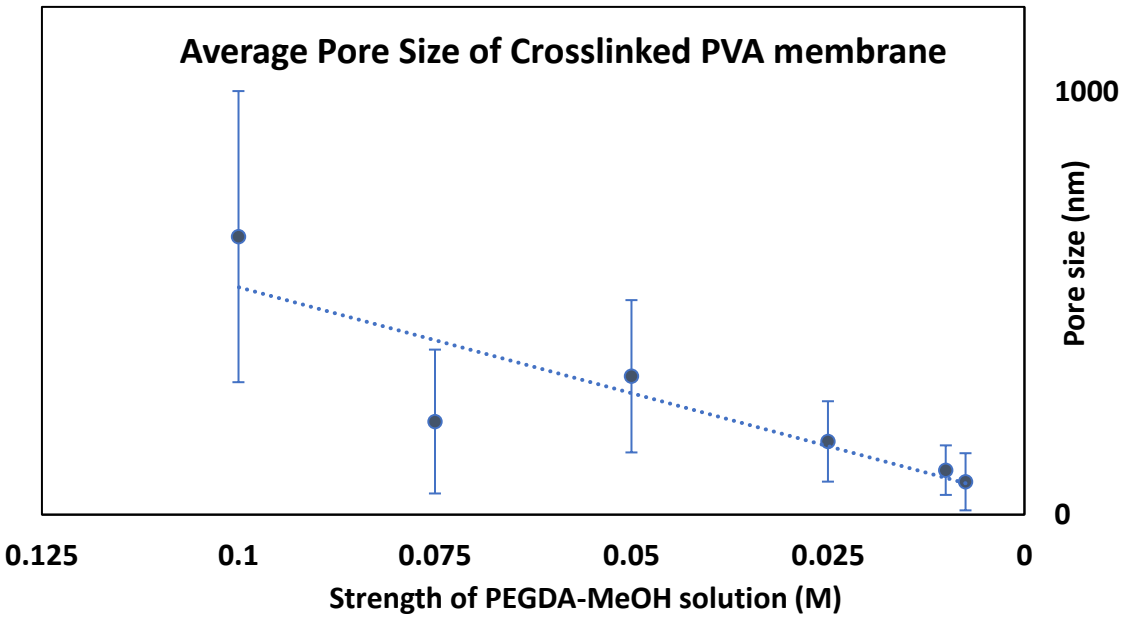

Figure 14. Effect of crosslinker concentration (0.1M – 0.0075M) on the average pore size of crosslinked PVA membranes.

From Figure 13 and 14, it is seen that the crosslinking can be effectively done via an acid catalyzed esterification reaction for PVA nanofibrous mats. In the past, Li Yao et. al (2003) have physically crosslinked electrospun 100% hydrolyzed PVA fibers using methanol treatment. They found that methanol serves to increase the degree of crystallinity and therefore, the number of physical crosslinks in the electrospun PVA fibers. Moreover, the physical crosslinks occur by removal of residual water within the PVA fibers by methanol, thus allowing PVA and water hydrogen bonding to be replaced with intermolecular PVA hydrogen bonding resulting in additional crystallization. This explains the stabilization of electrospun PVA fibers in water after the crosslinking.

In addition to the physical crosslinking, the PEGDA is assumed to form an ester carbonyl bond and covalently crosslinking the sample. The varying pore sizes across the

PVA mat can be attributed to this reaction appearing as fusion points through the membrane. Furthermore, the appearance of these fusion points decreases when the crosslinker strength is decreased. This also explains the improvement in surface morphology of crosslinked membranes at lower concentration of PEGDA and stabilization due to greater contribution from methanol. In conclusion, the above discussed method establishes a protocol that allows to tune the porosity of the crosslinked PVA membranes and the co-spun mats and in future can be useful while fabricating hydrophilic membranes for UF or MF applications.

Modified Dual Electrospinning

Based on the elemental map developed from the EDS analysis for dual electrospinning, the control setup was modified to facilitate uniform deposition of PVA and PVC on the co-spun mat prior to filtration experiments. The PVA syringe was fitted with a 3-way adapter to provide gas assisted (8-10 psi) electrospinning. The gas was introduced with the assumption that the fiber deposition would be uniform and dispersed on the entire surface of the rotary drum. The PVC syringe was placed perpendicular to the rotary drum at an elevation of 5 cm from the ground. This was done to ensure PVC fibers directly deposit on the drum as opposed to collecting on the ground surface. From the controlled experiments, it was observed that when the PVA syringe fitted with gas kept on the opposite side and in-line with PVC syringe, the gas would interfere with the deposition of PVC fibers or would dry the PVC solution on the tip of the needle disabling PVC electrospinning. Therefore, the PVA syringe was kept at an angle of 45° above the rotary drum. Figure 15 shows the modified dual electrospinning setup.

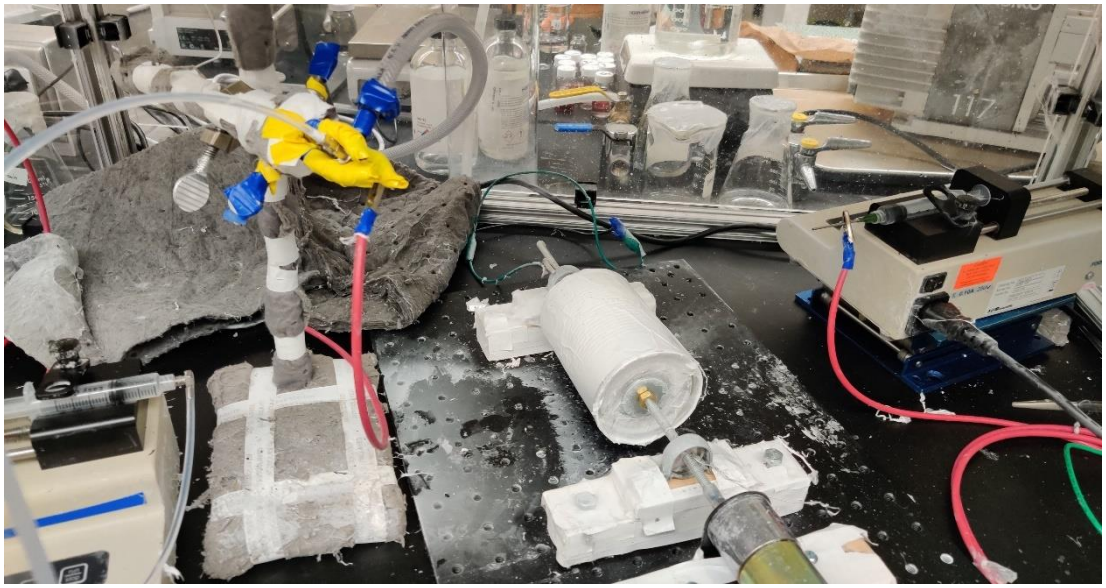

Figure 15. Modified dual electrospinning setup.

Prior to performing filtration experiments and tensile tests, the modified dual electrospinning arrangement was used to electrospun 3 membrane mats. For these membranes, PVC flow rates were kept constant and PVA flow rates were varied to study the impact of hydrophilicity on the performance of these membranes. Specifically, the co-spun mats were fabricated with a mass flow ratio (PVA/PVC) of 1.8, 1.4 and 0.9, and were labeled as M-1, M-2 and M-3, respectively. Furthermore, all the 3 co-spun mats were crosslinked with the 0.0075M PEGDA-MeOH solution.

Membrane Filtration Test

In order to assess the membrane flux, dead-end cell filtration experiments were performed with ultrapure water. The filtration experiments were conducted at 5.7 psi pressure for all the prepared co-spun mats and a crosslinked PVA (CL-PVA) mat shown in Figure 16. All the membranes showed a higher flux values, and an increase in the flux values was observed with lower mass flow ratio mats (M3 > CL-PVA > M2 > M1). The water flux for the CL – PVA mat was found to be 155 L m^{-2} h^{-1} psi^{-1}, suggesting that these

membranes are very porous. Furthermore, it was expected that with the increase of hydrophilic polymer on the membrane surface would increase the water flux through them. However, the reported flux for M-1 was found to be low at 6.8 L m^{-2} h^{-1} psi^{-1} in comparison to the other mats even though it has the highest amount of PVA deposited. Additionally, at a lower mass flow ratio (M-2) the water flux increased, and for M-3 with the least mass flow ratio the flux increased significantly.

The decrease in flux value for the mat with the most PVA content can be attributed to the changes in surface morphology and the pore creation on crosslinking of PVA. At higher mass flow ratios of PVA, there exists more amount of PVA on the surface and dense layers of the nanofibrous mats. With the crosslinking reaction, wherein, PVC fibers are unaffected and the PVA mat crosslinks constricting the PVC fibers between them (Figure 17a). The non-woven PVC fibers on the surface and bottom layers are constricted by several layers of crosslinked PVA. This finding was further substantiated by taking a SEM mage of the crosslinked co-spun mat shown in Figure 17a. The PVC fibers appear weaved inside the crosslinked PVA layer giving a denser structure to the co-spun mat and thus, having lower flux values.

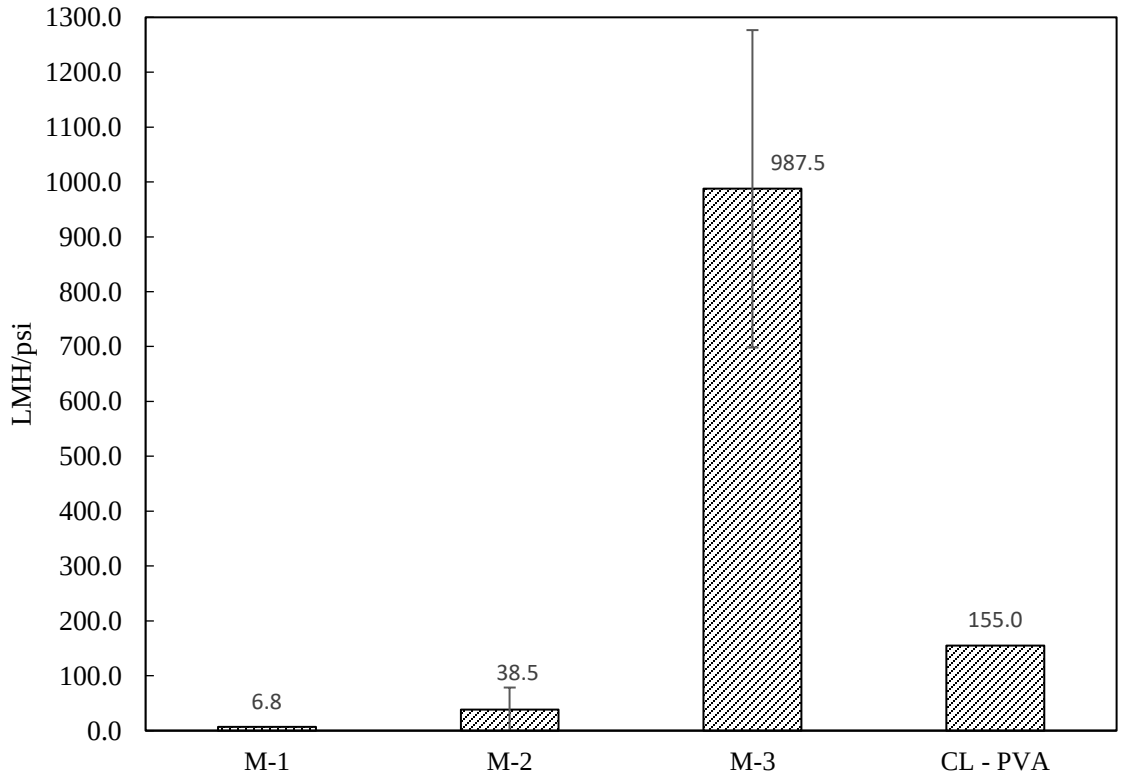

Figure 16. Water flux (LMH/psi) for the crosslinked PVA and co-spun mats collected of the dead-end cell filtration setup.

For the case of M-2, the data was collected from two different locations in the same co-spun mat. The increased flux values can be attributed to the fact that these mats were electrospun with a lower mass flow ratio of PVA. The presence of lower PVA concentration results in a less dense or a more porous structure. Moreover, an SEM image (Figure 17b) of the M-2 revealed that the deposition of PVA and PVC fibers were inconsistent despite the modified electrospinning setup. PVA was easily detected in the co-spun mat from the crosslinked patches, whereas the PVC appeared as their characteristic rigid fibers. This substantiates for the variations observed in the flux values for two different membrane location in the same co-spun mat, wherein, the higher flux can be

attributed to the locations where deposited PVC fibers and are surrounded with no or minimal crosslinked PVA fibers.

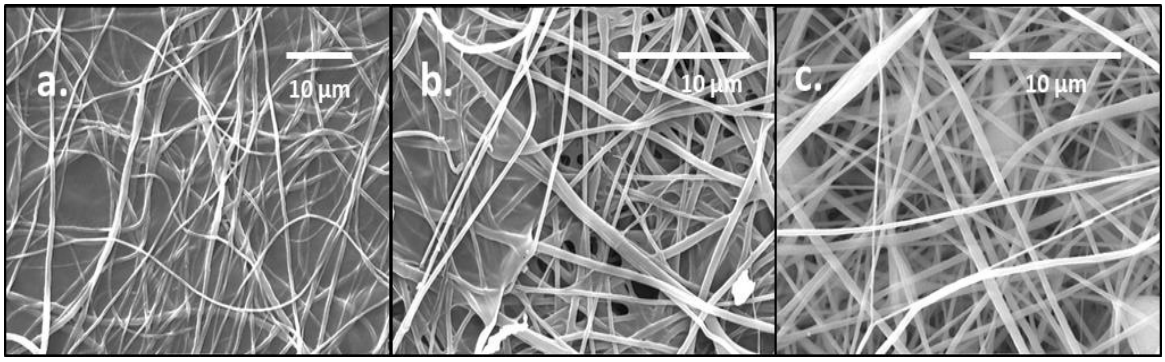

Figure 17. Crosslinked morphologies of the co-spun mats showing – (a) Weaved PVC fibers in crosslinked PVA layer (M-1), (b) Partially crosslinked PVA fibers with visible loose PVC fibers creating a porous structure (M-2), (c) A PVC fiber patch in the co-spun mat giving very porous membranes with high flux values (M-3).

Similarly, for M-3, the high flux values suggest that these mats had partial deposition of PVC and PVA across the membrane surface giving them a very porous structure or can be attributed to rupturing of the co-spun mat due to applied pressure. Thus, the results from the filtration test suggests that despite the increased PVA content the flux values decreased because of the denser morphologies created at higher mass flow ratios of PVA/PVC. To further understand the effect of increased hydrophilicity with PVA content, future experimentation will focus on challenging these membranes with salt passage and anti-fouling performance studies after achieving uniform deposition of PVA and PVC polymers.

Tensile Testing

In order to verify and attest that the crosslinking reaction imparted mechanical strength and durability to the co-spun mats, the prepared mats were subjected to tensile test to pulling them until failure and generating stress-strain plots (Figure 18). For the crosslinked PVA (CL-PVA) mats, a dramatic increase in the Young's Modulus (0.08 MPa) was observed much higher than the as-spun PVA fibers and the crosslinked PVA previously reported by Quinn et. al (2018). These results further substantiate the fact that the PVA in the co-spun mats have crosslinked successfully. Additionally, the crosslinker length used in this study has been previously (Quinn et al, 2018) shown to have a positive impact on the tensile strength of crosslinked PVA membrane in a previous study. More importantly, CL-PVA were able to withstand higher stresses and higher strains indicative of their ductile behavior and higher material strength.

On increasing the PVA content of the co-spun mats and in comparison, to the CL-PVA, at higher mass flow ratios M-1, the Young Moduli increased by approximately 1050 %, and 475% and 137% for M-2 and M-3, respectively. This data suggests that the integration of PVC fibers with crosslinked PVA layer gives the co-spun mat a higher yield strength. The co-spun mats with more PVA content are stiffer and stronger making them desirable to be used for filtration. In addition, the co-spun mat is stronger because of the contribution of rigid PVC fibers. Also, these findings corroborate the results from filtration experiments, wherein, the highest mass flow ratio mat behaved as a denser membrane giving low flux values. The dense structure of these membranes further enhances their mechanical properties. Although, the crosslinked PVA mat possesses a lower yield strength

seen in Figure 18, the blend of varying amounts of PVA with PVC appreciably improves the yield strength of the co-spun mats.

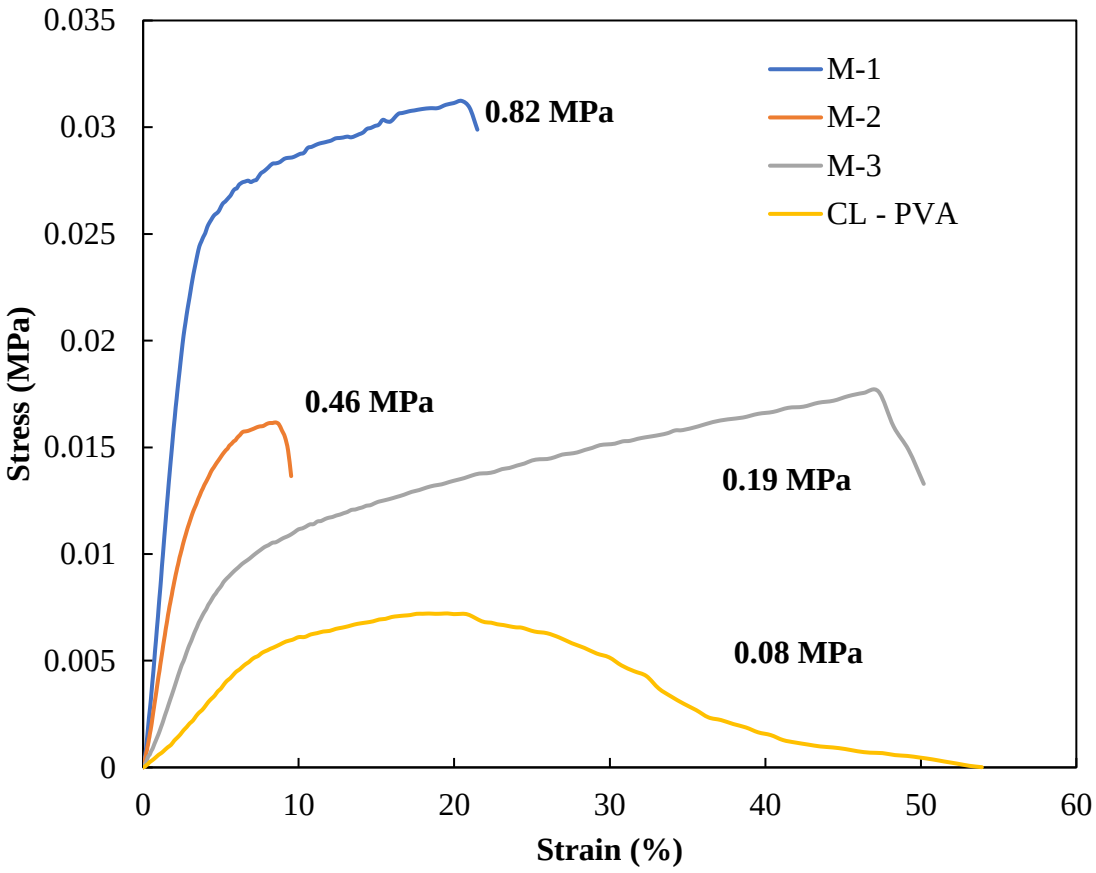

Figure 18. Stress vs strain plots for crosslinked co-spun M-1, M-2, M-3 and PVA mats labelled with Young's Modulus (E)

Interestingly, the co-spun mats M-2 and M-3 display similar ultimate tensile strength of 16 KPa, however, M-3 reaches at a higher strain percent. This can be attributed to the non-uniform deposition of PVA and PVC on the co-spun mat, wherein, M-3 having inconsistencies in deposition of PVC. Overall, the trend in the increase of their tensile

suggests that introducing more PVA to the co-spun mat will yield stronger membranes. Additionally, with consistent deposition of PVA and PVC, it is expected that these membranes will display even better mechanical characteristics.

CHAPTER 5

CONCLUSION AND FUTURE WORK

In summary, this work discusses a method to fabricate electrospun pretreatment membrane by blending two polymer solution into a nonwoven membrane comprised of fibers ~100 nm - 10 µm in diameter. Electrospinning conditions for hydrophobic polymer (PVC) and hydrophilic polymer (PVA) were established prior to dual spinning them on a rotary drum collector. Furthermore, membrane characterization tests (SEM, EDX, FTIR and Confocal fluorescence microscopy) performed on the fabricated mats confirmed the presence of both polymers on the co-spun mat. Electrospinning deposits nanofibers in a seemingly random manner, therefore a rigorous analysis method was developed to map the relative composition of PVA and PVC on the membrane surface using EDS analysis. Based on this analysis, it was found that there exist inconsistencies in the mass deposition of both polymers suggesting an improvement in the control setup in order to establish a meaningful correlation between varying PVA concentration and tunable hydrophilicity.

Additionally, electrospun PVA mats was crosslinked with PEGDA-MeOH solution to impart mechanical strength and ensure their durability in filtration application. Interestingly, lowering the strength of the crosslinker improved the surface morphology of the membrane and significantly reduced the pore size of the crosslinked mats. On further investigation, it was found that the pore size of the resulting crosslinked mats could be tuned by varying the strength of the crosslinker. Therefore, gaining control over the porosity of a hydrophilic membrane during the crosslinking reaction can provide desirable membrane characteristics such as high solute rejection, fouling resistance and permeability.

Furthermore, the ability to tailor the porosity of these membranes further corroborates the hypothesis of fabricating tunable pretreatment membranes.

After establishing the protocol for fabricating and crosslinking the co-spun mats, membranes with different mass flow ratio of PVA/PVC were electrospun with a modified setup keeping the PVC flow constant. Filtration experiments revealed a negative correlation between the PVA content and the flux, because of the dense membrane structure resulting from constriction of PVC fibers in the crosslinked PVA fibers. Although, it was hypothesized that increasing the PVA concentration would lead to a higher flux, however, it is expected that in-spite of the decreasing flux, the co-spun mats would display a positive correlation with flux when exposed to fouling conditions due to their hydrophilicity. Additionally, on subjecting these membranes to tensile test, the co-spun mats with high mass flow ratio performed extremely well than the only crosslinked PVA membrane, wherein the Young Moduli increased by 1060%. In summary, membrane fabrication via electrospinning, a relatively easy and scalable technique possessing tunable characteristics and durable membrane performance points towards their potential application as UF/MF pretreatment for RO systems.

Future work for this study includes gas assisted electrospinning for both polymer solutions to achieve a more disperse and uniform composition of each on the co-spun mats. Furthermore, modifying the control setup with an automatic slider with to and fro movement for consistencies in the mass deposition rate. This would allow to establish the effect of PVA content with hydrophilicity and build a correlation of hydrophilicity with an electrospinning-controlled variable. The next steps would be to perform anti-fouling performance tests to substantiate the hypothesis of preventing fouling with hydrophilic

membranes. Besides experimental modification, introducing functional groups on PVA such as to facilitate selective removal of heavy metal atoms.

REFERENCES

Service RF. Desalination freshens up. Science 2006;313:1088- 1090

Greenlee, L. F., Lawler, D. F., Freeman, B. D., Marrot, B., Moulin, P., & Ce, P. (2009). Reverse osmosis desalination : Water sources , technology , and today ' s challenges. *Water Research*, *43*(9), 2317–2348. https://doi.org/10.1016/j.watres.2009.03.010

Gleick PH. The world's water, 2006-2007: the biennial report on freshwater resources. Washington, DC: Island Press; 2006.

Semiat R. Energy issues in desalination processes. Environ Sci Tech- nol 2008;42:8193–201.

Anderson MA, Cudero AL, Palma J. Capacitive deionization as an electrochemical means of saving energy and delivering clean water. Comparison to present desalination practices: will it compete? Electrochim Acta 2010;55:3845–56

Wolfe, P., 2005. Fujairah Marks Major Milestone for Desalination in Middle East. Water and Wastewater International. Available from: http://ww.pennnet.com/display_article/227597/20/ ARTCL/none/none/1/Fujairah-marks-major-milestone-for- desalination-in-Middle-East

Lin, L., Feng, C., Lopez, R., Coronell, O., 2016. Identifying facile and accurate methods to measure the thickness of the active layers of thin-film composite membranes - a comparison of seven characterization techniques. J. Membr. Sci. 498:167–179. http://dx.doi.org/10.1016/j.memsci.2015.09.059.

Ochando-Pulido, J.M., Víctor-Ortega, M.D., Martínez-Ferez, A., 2016.Membrane fouling in- sight during reverse osmosis purification of pretreated olive mill wastewater. Sep. Purif. Technol. 168:177–187. http://dx.doi.org/10.1016/j.seppur.2016.05.024

Tang, F., Hu, H.Y., Sun, L.J., Sun, Y.X., Shi, N., Crittenden, J.C., 2016b. Fouling characteristics of reverse osmosis membranes at different positions of a full-scale plant for munici- pal wastewater reclamation. Water Res. 90:329–336. http://dx.doi.org/10.1016/j. watres.2015.12.028.

Werber, J. R., Osuji, C. O., & Elimelech, M. (2016). Materials for next-generation desalination and water purification membranes. *Nature Reviews Materials*, *1*(April). https://doi.org/10.1038/natrevmats.2016.18

Lee, K. P., Arnot, T. C., & Mattia, D. (2011). A review of reverse osmosis membrane materials for desalination-Development to date and future potential. *Journal of Membrane Science*, *370*(1–2), 1–22. https://doi.org/10.1016/j.memsci.2010.12.036

Kang, G. dong, & Cao, Y. ming. (2012). Development of antifouling reverse osmosis membranes for water treatment: A review. *Water Research*, *46*(3), 584–600. https://doi.org/10.1016/j.watres.2011.11.041

Bartels, C., Franks, R., Rybar, S., Schierach, M., Wilf, M., 2005. The effect of feed ionic strength on salt passage through reverse osmosis membranes. Desalination 184, 185–195.

Choi, S., Zuwhan, Y., Hong, S., Ahn, K., 2001. The effect of co- existing ions and surface characteristics of nanomembranes on the removal of nitrate and fluoride. Desalination 133, 53–64.

Hilal, N., Al-Zoubi, H., Darwish, N.A., Mohammad, A.W., Abu Arabi, M., 2004. A comprehensive review of nanofiltration membranes: treatment, pretreatment, modelling, and atomic force microsopy. Desalination 170,281-308

Li, D., & Wang, H. (2010). *Recent developments in reverse osmosis desalination membranes †*. 4551–4566. https://doi.org/10.1039/b924553g

Baker, R.W., 2004. Membrane Technology and Applications. John Wiley & Sons, Ltd., Chichester.

Lonsdale, H.K., Merten, U., Riley, R.L., 1965. Transport properties of cellulose acetate osmotic membranes. Journal of Applied Polymer Science 9, 1341–1362.

Merten, U., 1963. Flow relationships in reverse osmosis. Industrial and Engineering Chemistry Fundamentals 2 (3), 229–232.

Paul, D.R., 1972. The role of membrane pressure in reverse osmosis. Journal of Applied Polymer Science 16, 771–782.

Wijmans, J.G., Baker, R.W., 1995. The solution-diffusion model: a review. Journal of Membrane Science 107, 1–21.

Morenski, F., 1992. Current pretreatment requirements for reverse osmosis membrane applications. In: Official Proceedings of the 53rd International Water Conference, pp. 325–330.

Wilf, M., Klinko, K., 2001. Optimization of seawater RO systems design. Desalination 138, 299–306.

Kim, S., Hoek, E.M.V., 2005. Modeling concentration polarization in reverse osmosis processes. Desalination 186, 111–128.

Song, L.F., Elimelech, M., 1995. Theory of concentration polarization in cross-flow filtration. Journal of the Chemical Society-Faraday Transactions 91 (19), 3389–3398.

Bacchin, P., Si-Hassen, D., Starov, V., Clifton, M.J., Aimar, P., 2002. A unifying model for concentration polarization, gel-layer formation and particle deposition in cross-flow membrane filtration of colloidal suspensions. Chemical Engineering Science 57, 77–91.

Gekas, V., Hallstro¨m, B., 1987. Mass transfer in the membrane concentration polarization layer under turbulent cross flow I. Critical literature review and adaptation of existing sherwood correlations to membrane operations. Journal of Membrane Science 30, 153–170

Sutzkover, I., Hasson, D., Semiat, R., 2000. Simple technique for measuring the concentration polarization level in a reverse osmosis system. Desalination 131, 117–127.

Zydney, A.L., 1997. Stagnant film model for concentration polarization in membrane systems. Journal of Membrane Science 130, 275–281.

Penña, N., Gallego, S., del Vigo, F., & Chesters, S. P. (2013). Evaluating impact of fouling on reverse osmosis membranes performance. *Desalination and Water Treatment*, *51*(4–6), 958–968. https://doi.org/10.1080/19443994.2012.699509

Al-Amoudi, A.S., 2010. Factors affecting natural organic matter (NOM) and scaling fouling in NFmembranes: a review. Desalination 259:1–10. http://dx.doi.org/10.1016/j.desal. 2010.04.003.

Eric, M.V., Seungkwan, H., Menachem, E., 2001. Influence ofmembrane surface properties on initial rate of colloidal fouling of reverse osmosis and nanofiltration membranes. J. Membr. Sci. 188:115–128. http://dx.doi.org/10.1016/S0376-7388(01)00376-3

Kochkodan, V., Johnson, D.J., Hilal, N., 2014. Polymeric membranes: surface modification for minimizing (bio)colloidal fouling. Adv. Colloid Interf. Sci. 206:116–140. http:// dx.doi.org/10.1016/j.cis.2013.05.005.

Tang, C.Y., Chong, T.H., Fane, A.G., 2011. Colloidal interactions and fouling of NF and RO membranes: a review. Adv. Colloid Interf. Sci. 164:126–143. http://dx.doi.org/10.1016/j.cis.2010.10.007.

Giglia, S., Straeffer, G., 2012. Combinedmechanism fouling model andmethod for optimization of series microfiltration performance. J. Membr. Sci. 417–418:144–153. http://dx.doi.org/10.1016/j.memsci.2012.06.026.

Lee, K.C., Beak, H.J., Choo, K.H., 2015b. Membrane photoreactor treatment of 1,4-dioxane- containing textile wastewater effluent: performance, modeling, and fouling control. Water Res. 86:58–65. http://dx.doi.org/10.1016/j.watres.2015.05.017.

Mirbagheri, S.A., Bagheri, M., Bagheri, Z., Kamarkhani, A.M., 2015. Evaluation and prediction of membrane fouling in a submerged membrane bioreactor with simultaneous upward and downward aeration using artificial neural network-genetic algorithm. Process Saf. Environ. Prot. 96:111–124. http://dx.doi.org/10.1016/j.psep.2015.03.015.

Tan, Y.Z., Chew, J.W., Krantz, W.B., 2016. Effect ofhumic-acid fouling onmembrane distil- lation. J. Membr. Sci. 504:263–273. http://dx.doi.org/10.1016/j.memsci.2015.12.051

Jiang, S., Li, Y., & Ladewig, B. P. (2017). A review of reverse osmosis membrane fouling and control strategies. *Science of The Total Environment*, *595*, 567–583. https://doi.org/10.1016/J.SCITOTENV.2017.03.235

Valavala, R., Sohn, J., Han, J., Her, N., & Yoon, Y. (2011). *Pretreatment in Reverse Osmosis Seawater Desalination : A Short Review*. *16*(4), 205–212.

Jamaly, S., Darwish, N. N., Ahmed, I., & Hasan, S. W. (2014). A short review on reverse osmosis pretreatment technologies. *Desalination*, *354*, 30–38. https://doi.org/10.1016/j.desal.2014.09.017

Sweetwater Technologies, Government Engineering. Available from: http://www.govengr.com/ArticlesNov06/potable.pdf

Gabelich CJ, Yun TI, Coffey BM, Suffet IH. Effects of alumi- num sulfate and ferric chloride coagulant residuals on poly- amide membrane performance. Desalination 2002;150:15- 30

Brehant A, Bonnelye V, Perez M. Comparison of MF/UF pretreatment with conventional filtration prior to RO mem- branes for surface seawater desalination. Desalination 2002;144:353-360.

Pearce GK. The case for UF/MF pretreatment to RO in sea- water applications. Desalination 2007;203:286-295

Cote, P., Cadera, J., Coburna, J., & Alistair, M. (2001). *A new immersed membrane for pretreatment to reverse osmosis*. *139*(May), 229–236.

Brehant, A., Bonnelye, V., Perez, M., 2003. Assessment of ultrafiltration as a pretreatment of reverse osmosis membranes for surface seawater desalination. Water Science and Technology: Water Supply 3 (5–6), 437–445.

Bu-Rashid, K.A., Czolkoss, W., 2007. Pilot tests of multibore UF membrane at Addur SWRO desalination plant, Bahrain. Desalination 203, 229–242.

Kamp, P.C., Kruithof, J.C., Folmer, H.C., 2000. UF/RO treatment plant Heemskerk: from challenge to full scale application. Desalination 131, 27–35.

Teuler, A., Glucina, K., Laıˆne´ , J.M., 1999. Assessment of UF pretreatment prior RO membranes for seawater desalination. Desalination 125, 89–96.

Tiwari, S.A., Goswami, D., Prabhakar, S., Tewari, P.K., 2006. Assessment of an ultrafiltration pre-treatment system for a seawater reverse osmosis plant. International Journal of Nuclear Desalination 2 (2), 132–138.

Xu, J., Ruan, G., Chu, X., Yao, Y., Su, B., Gao, C., 2007. A pilot study of UF pretreatment without any chemicals for SWRO desalination in China. Desalination 207, 216–226.

Bonnélye, V., Guey, L., Del Castillo, J., 2008. UF/MF as RO pre-treatment: the real benefit. Desalination 222:59–65. http://dx.doi.org/10.1016/j.desal.2007.01.129

Teng, C.K., Hawlader, M.N.A., Malek, A., 2003. An experiment with different pretreatment methods. Desalination 156:51–58. http://dx.doi.org/10.1016/S0011-9164(03)00324- 2.

Zhang, J.D., Liu, Y.W., Gao, S.M., Li, C.Z., Zhang, F., Zen, H.M., Ye, C.S., 2006a. Pilot testing of outside-in UF pretreatment prior to RO for high turbidity seawater desalination. De- salination 189:269–277. http://dx.doi.org/10.1016/j.desal.2005.07.009.

Bae, H., Kim, H., Jeong, S., Lee, S., 2011. Changes in the relative abundance of biofilm-forming bacteria by conventional sand-filtration andmicrofiltration as pretreatments for seawater reverse osmosis desalination. Desalination 273:258–266. http://dx.doi. org/10.1016/j.desal.2010.12.030.

Bartels, C., Rybar, S., Franks, R., 2006. Integrated membrane desalination systems – potential benefits of combined technology. Hydranautics Available from: http://www. membranes.com/docs/papers/New%20Folder/ Gulf%20Industry%20Magazine%20-%20Hydranautics.pdf

Quinn, J. A., Yang, Y., Buffington, A. N., Romero, F. N., & Green, M. D. (2018). Preparation and characterization of crosslinked electrospun poly(vinyl alcohol) nanofibrous membranes. *Polymer*, *134*, 275–281. https://doi.org/10.1016/j.polymer.2017.11.023

Hong, H., Tronstard, Z., Yang, Yi., & Green, M. D (2018). Characterization of PVC-soy Protein Nonwoven Mats prepared by Electrospinning. *AIChE J* , 64: 2737–2744, 2018 https://doi.org/10.1002/aic.16109

Tarus, B., Fadel, N., Al-oufy, A., & El-messiry, M. (2016). Effect of polymer concentration on the morphology and mechanical characteristics of electrospun cellulose acetate and poly (vinyl chloride) nanofiber mats. *Alexandria Engineering Journal*, *55*(3), 2975–2984. https://doi.org/10.1016/j.aej.2016.04.025

Mit-uppatham C, Nithitanakul M, Supaphol P. Ultrafine electrospun polyamide-6 fibers: effect of solution conditions on morphology and average fiber diameter. Macromol Chem Phys 2004;205:2327–38.

Taylor, G., & A, P. R. S. L. (1969). *Electrically Driven Jets*. 453–475. https://doi.org/10.1098/rspa.1969.0205

Finch, C. A., Poly(vinyl alcohol): Properties and Applications; Wiley: New York, 1973.

N. Hilal, O. O. Ogunbiyi, N. J. Miles and R. Nigmatullin, Sep. Sci. Technol., 2005, 40, 1957–2005.

A. G. Fane and C. J. D. Fell, Desalination, 1987, 62, 117–136.

A. Nabe, E. Staude and G. Belfort, J. Membr. Sci., 1997, 133, 57–72.

Miller J, Dreyer D, Bielawski C, Paul D, Freeman B (2017). Surface Modification of Water Purification membrane. Angew. Chem. Int. Ed. 10.1002/anie.201601509

Otitoju, T. A., Ahmad, A. L., & Ooi, B. S. (2018). Recent advances in hydrophilic modification and performance of polyethersulfone (PES) membrane via additive blending. *RSC Advances*, *8*(40), 22710–22728. https://doi.org/10.1039/c8ra03296c

Bhardwaj, N., & Kundu, S. C. (2010). *Electrospinning : A fascinating fi ber fabrication technique*. *28*, 325–347. https://doi.org/10.1016/j.biotechadv.2010.01.004

Zhang X, Chen Y, Konsowa AH, Zhu X, Crittenden JC. Evaluation of an innovative polyvinyl chloride (PVC) ultrafiltration membrane for wastewater treatment. Separation and Purification Technology. 2009;70(1):71-78

Dong W, Ruan X, Ni Z, Chen M. Influence of soy protein isolate on the thermal stability of poly(vinyl chloride) in the presence or absence of calcium and zinc stearates. Polymer Degradation and Stability, 2013;98(1):96-101.

Ren, G., Xu, X., Liu, Q., Cheng, J., Yuan, X., Wu, L., & Wan, Y. (2006). Electrospun poly (vinyl alcohol)/glucose oxidase biocomposite membranes for biosensor applications. Reactive and Functional Polymers, 66(12), 1559-1564.

APPENDIX A

2^3 FULL FACTORIAL DESIGN FOR 12% PVA AND 15% PVC SOLUTIONS

A1.1 2^3 Full factorial runs for 12% PVA solution

Factors				Low (-1)	High (+1)	
A = Flow rate			**A**	0.75	1.5	**ml/hr**
B = Applied voltage			**B**	18	23	**kV**
C = Tip to collector distance			**C**	12	15	**cm**
Run no.	**A**	**B**	**C**	**Fiber Diameter**	**Standard Deviation**	**Temp**	**Humidity**
				(nm)	**(nm)**		
1	0.75	18	12	168	39		
2	1.5	18	12	182	62	23.5	30%
3	0.75	23	12	182	41	23.5	29%
4	1.5	23	12	181	61	23.8	30%
5	0.75	18	15	155	41	23.9	31%
6	1.5	18	15	148	34	23.5	30%
7	0.75	23	15	174	65	22.9	30%
8	1.5	23	15	181	47	22.4	33%

Table A1. Average fiber diameter and standard deviation obtained from DOE runs for 12% PVA solutions.

A1.2 Scanning electron micrographs for 12% PVA DOE runs from Table A1

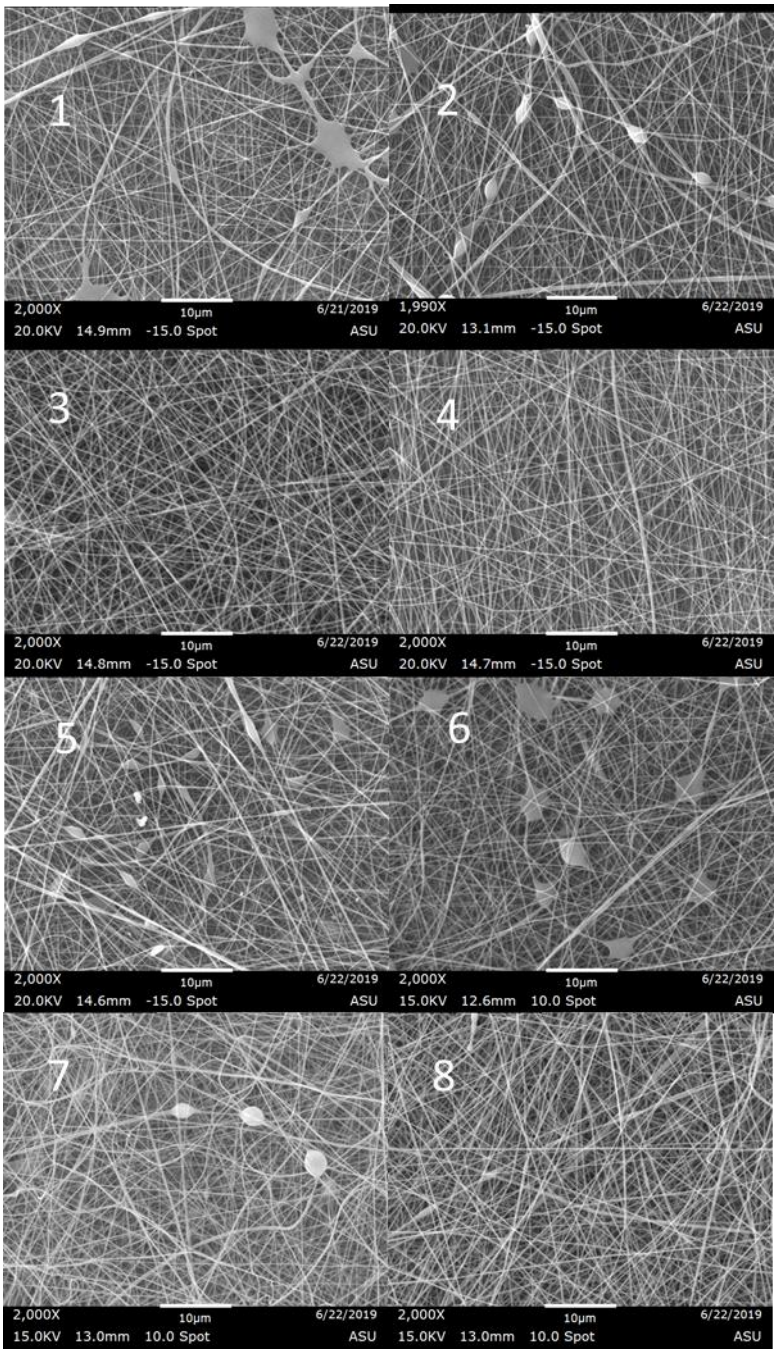

A.1.3 Pareto plot for 12% PVA solution

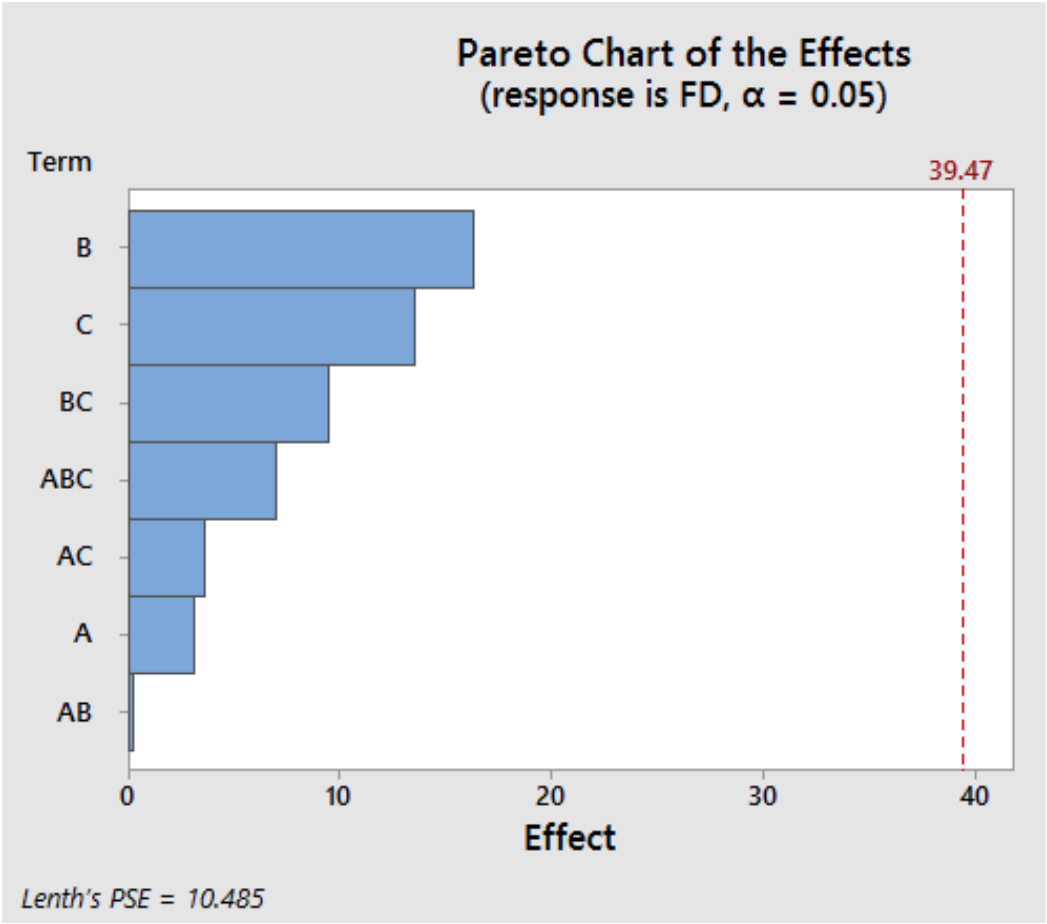

Alias Structure

Factor	Name
A	Flow Rate
B	Applied Voltage
C	T/C distance

A2.1 2^3 Full factorial runs for 15% PVC solution.

Factors					Low (-1)	High (+1)	
A = Flow rate				**A**	0.5	1	**ml/hr**
B = Applied voltage				**B**	12	18	**kV**
C = Tip to collector distance				**C**	12	15	**cm**
Run no.	**A**	**B**	**C**	**Fiber Diameter**	**Standard Deviation**	**Temp**	**Humidity**
				(nm)	**(nm)**		
1	0.5	12	12	289	109	22.5°C	24.50%
2	1	12	12	298	151	22.4°C	24.40%
3	0.5	18	12	350	129	22.5°C	25%
4	1	18	12	296	148	22.3°C	24%
5	0.5	12	15	347	189		
6	1	12	15	**468**	359	22.3°C	25%
7	0.5	18	15	**264**	127	22.5°C	25%
8	1	18	15	380	154	22.3°C	24.80%

Table A. Average fiber diameter and standard deviation obtained from DOE runs for 15% PVC solutions.

A2.2 Scanning electron micrographs for 15% PVC DOE from Table A2

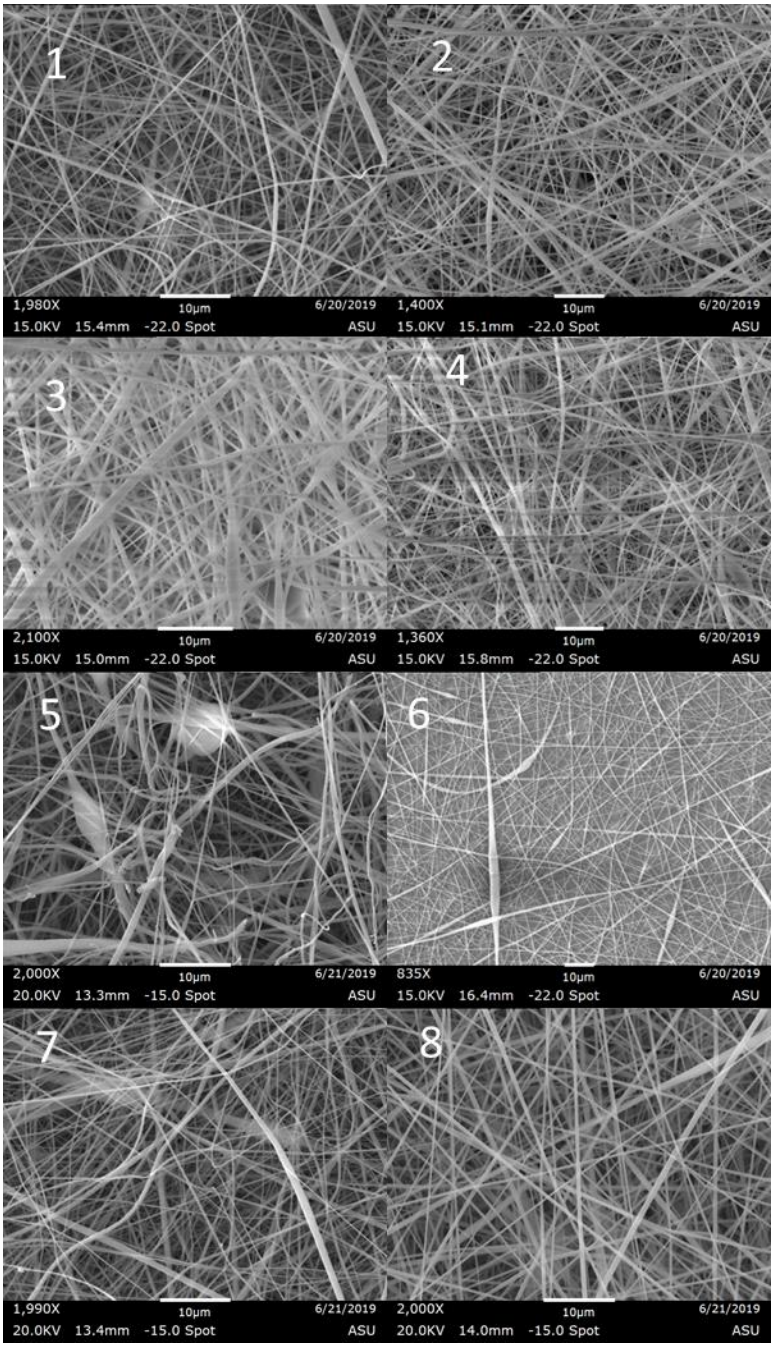

A.2.3 Pareto plot for 15% PVC solution

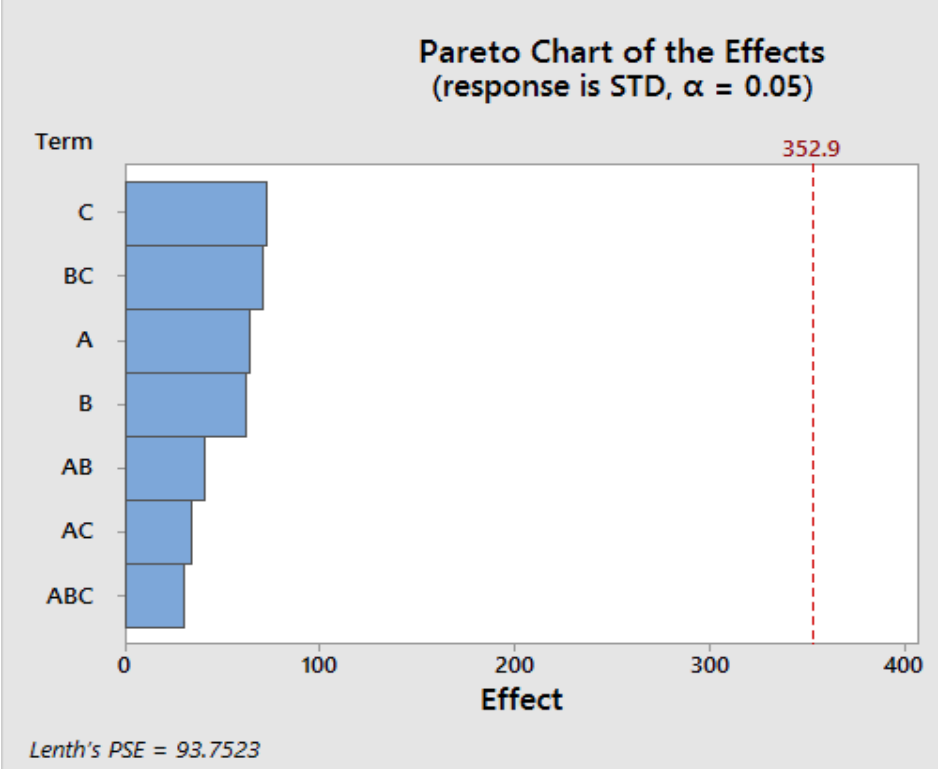

Alias Structure

Factor	Name
A	Flow rate
B	Applied voltage
C	T/C distance